Combustion and Flame 272 (2025) 113875

Contents lists available at ScienceDirect

Combustion and Flame

journal homepage: www.sciencedirect.com/journal/combustion-and-flame

High-pressure conversion of ammonia additivated with dimethyl ether in a flow reactor

Pedro García-Ruiz, Pablo Ferrando, María Abián, María U. Alzueta *

Aragón Institute of Engineering Research (I3A), Department of Chemical and Environmental Engineering, University of Zaragoza, 50018 Zaragoza, Spain

ARTICLE INFO

Keywords:
Ammonia
Dimethyl ether
Flow reactor
high-pressure
N2O
Kinetic modeling

ABSTRACT

The oxidation of ammonia (NH_3) mixed with dimethyl ether (DME) was investigated from experimental and modeling points of view using a quartz flow reactor with argon as bath gas from 350 K to 1225 K, for two different DME/NH_3 ratios (0.05 and 0.3), three oxygen excess ratios ($\lambda = 0.7$, 1 and 3) and various pressures (1, 10, 20 and 40 bar).

The effect of pressure, oxygen stoichiometry, temperature, and DME/NH_3 ratio has been analyzed on DME, NH_3, NO, NO_2, N_2O, N_2, O_2, H_2, HCN, CH_4, CO, and CO_2 concentrations.

The present study indicates that oxygen availability, DME/NH_3 ratio, and pressure are important variables that shift NH_3 and DME conversion to lower temperatures as their values increase. Under certain conditions, the pressure effect can avoid NO and HCN production, which would represent a benefit for pressure applications.

The main products of ammonia/dimethyl ether oxidation are N_2, N_2O, CO, and CO_2, and under certain conditions, NO, H_2, CH_4, and HCN are also produced. NO_2 is always detected below 5 ppm for all the conditions considered. The N_2O formation is favored by increasing the O_2 stoichiometry, pressure, and/or DME/NH_3 ratio.

The experimental results are interpreted and discussed in terms of an updated detailed chemical kinetic mechanism, which captures, with a general good agreement, the main trends of NH_3 and DME conversion under the considered conditions. Despite this, some calculated species present discrepancies with the experimental results. The main challenge is the consideration of the C-N interactions that can be present in the combustion of DME/NH_3 mixtures.

1. Introduction

Climate change mitigation and the energy transition to minor carbon dioxide and harmful pollutant emissions require the use of fuels with lower carbon content. This approach is making ammonia more and more interesting as a carbon-free fuel because it is one of the major chemicals produced in the world and presents a mature production, storage, and transportation infrastructure [1]. Besides, NH_3 can ideally be burned to produce N_2 and H_2O with zero CO_2 production through the reaction $4NH_3 + 3O_2 \rightleftharpoons 2N_2 + 6H_2O$ (r1). Additionally, under certain conditions, NH_3 can reduce NO emissions, when present, within the combustion chamber, leading to the production of N_2, through the non-catalytic selective reduction (SNCR) process [e.g. 2].

However, compared to conventional fossil fuels, ammonia has some drawbacks for its implementation such as low reactivity, and high autoignition temperature [e.g. 3]. One possible way to overcome these problems is mixing ammonia with other fuels. Experimental and simulation results of the combustion properties of pure ammonia [e.g. 4, 5] and its mixtures with hydrogen (H_2) [e.g. 6–8], methane (CH_4) [e.g. 9,10] and alcohols such as methanol (CH_3OH) [e.g. 11,12] and ethanol (C_2H_5OH) [e.g. 12] are reported in the literature. The authors noted that the combustion properties of the ammonia mixtures are better than the combustion of pure ammonia under the same experimental conditions, supporting that mixing NH_3 with other fuels improves its combustion properties. In this point, we have considered oxygenated fuels due to their applicability in combustion engines [13] and their lower soot and NO_x emissions than conventional diesel [13–15].

Dimethyl ether (DME) is one of the most promising oxygenated fuels which presents excellent autoignition properties, high oxygen content, high cetane number (i.e., 55~60), and good miscibility with hydrocarbons and NH_3 [16]. Early oxidation of DME can contribute to lowering the onset temperature of NH_3 oxidation, which directly benefits its use in high-pressure applications. Even a small fraction of DME in the mixtures can provoke a noteworthy effect in NH_3 ignition delay time and

* Corresponding author.
E-mail address: uxue@unizar.es (M.U. Alzueta).

https://doi.org/10.1016/j.combustflame.2024.113875
Received 2 August 2024; Received in revised form 18 November 2024; Accepted 19 November 2024
Available online 6 December 2024

temperature because DME can generate OH free radicals at low temperatures and thus promote NH_3 conversion [17–19]. Dai et al. [17] indicated that NH_3 blended with 5 % DME is more effective in accelerating NH_3 combustion than 10 % H_2 or 50 % CH_4. For these reasons, DME represents an attractive combustion enhancer for making NH_3 a suitable fuel for pressure applications such as turbines.

In the literature, many studies have reported the benefits of the use of DME in spark-ignition and compression-ignition engines, including improved thermal efficiency, reduced pollutant emissions, and practically particle-free operation [13,15]. NH_3, despite its significant benefits, faces several barriers that must be overcome before it can be directly utilized. Ignition promoters, such as DME, may play a critical role in the NH_3 autoignition behavior, determining its potential use in engines and turbines [18]. This underlines the importance of increasing the experimental database with new studies addressing DME/NH_3 mixtures, which contributes to improve the development of new fuels and to adapt engine modifications to fuel properties.

DME combustion is known to exhibit a negative temperature coefficient (NTC) behavior that leads to two combustion regimes: one at low temperature, and another at high temperature [e.g. 19–24]. The NTC behavior takes place in the transition zone from the low to the high-temperature combustion regime. The starting temperature of the transition zone depends on the pressure and the mixture composition [25], and therefore it is important to study the combustion behavior of DME mixtures for different compositions under high-pressure conditions, as is performed in the present work.

In the literature, DME pyrolysis, oxidation, and its interaction with NO have been widely studied, in flow reactors under different pressure conditions (from 1 to 60 bar) [e.g. 21,24,26–29]. To a minor extent, oxidation of DME/NH_3 mixtures has also been studied using other experimental setups, such as a shock tube [e.g. 19], a constant-volume combustion vessel [e.g. 30], a rapid compression machine (RCM) [e.g. 17], a premixed burner [e.g. 31], a jet-stirred reactor (JSR) [e.g. 22], and a micro-flow reactor [32]. Also, different chemical kinetic mechanisms [e.g. 17,21,32–38] have been proposed for the oxidation of the mixtures.

Regarding DME/NH_3 concentration ratios, previous works in the literature covered a wide range of DME/NH_3 relationships, from low DME/NH_3 ratios (DME/NH_3 = 0.021 [e.g. 17]) in which DME can be considered as an additive, to higher ratios (DME/NH_3 = 1 [e.g. 18,19]) in which DME has the same or a comparable concentration of NH_3. However, none of them used a flow reactor setup. This frames the importance of studying different proportions of DME in the mixture, as is performed in the present work.

Pressure represents a critical variable in turbines and engines powered with NH_3, since increasing pressure can contribute to reduce NH_3 slip and NO emission, and it is crucial to examine if other reaction products follow the same behavior. Some previous studies considered the effect of pressure (from 5 to 100 bar) during the combustion of DME/NH_3 mixtures [e.g. 17–19]. Dai et al. [17] studied the ignition delay time of DME/NH_3 mixtures with DME/NH_3 ratios of 0.02 and 0.05, from reducing to oxidizing conditions (λ = 0.5, 1, and 2) in the 10 to 70 bar pressure range, and observed that for 2-5 % of DME in the fuel, the NH_3 ignition delay time (IDT) decreased more than an order of magnitude compared to pure NH_3 ignition. Issayev et al. [18] reported a laminar burning velocity (LBV) and ignition delay time study in a RCM from 20 to 40 atm and from reducing to oxidizing conditions (λ = 0.5, 1, and 2). The authors pointed out that DME/NH_3 = 1 shows a low-temperature combustion ignition behavior close to neat DME. In addition, they found an IDT pressure dependence for low DME/NH_3 ratios. Jiang et al. [19] studied the ignition delay time of a DME/NH_3 mixture under oxygen stoichiometric conditions in a shock tube, reporting the effect of fuel blending in the NTC behavior up to a pressure of 10 bar and comparing several kinetic models. They also concluded that the addition of DME also promotes NH_3 consumption.

Different kinetic models in the literature can, in general, reproduce IDT and LBV measurements [e.g. 17,18,36,38]. However, there are discrepancies between these models as Shi et al. [30] pointed out. A possible reason could be the interactions among DME and NH_3 and their respective derivatives. Examples of these interactions include the reactions: $CH_2O + NO \rightleftharpoons HCO + HNO$ (r2) and $CH_3 + NH \rightleftharpoons CH_2NH + H$ (r3), as pointed out by the recent work of Shi et al. [30].

As commented by Li et al. [39], there is a lack of studies about DME/NH_3 combustion at high pressure (P > 5 bar), especially in flow reactor setups in a variety of stoichiometries ranging from reducing to oxidizing atmospheres. In this context, the research of the present work aims to extend the knowledge of the oxidation behavior of DME/NH_3 mixtures under well-controlled conditions, by analyzing the effect of temperature (from 350 to 1225 K), pressure (from 1 to 40 bar), oxygen excess ratio (from reducing, λ = 0.7, to oxidizing conditions, λ = 3) and DME/NH_3 ratio (0.05, and 0.3).

Additionally, to shed light on chemical behavior and product species formation, the results are interpreted in terms of a chemical kinetic mechanism for DME/NH_3 mixtures, which has been compiled from the literature and updated in the present work.

2. Experimental methodology

Conversion of reactants and formed products during the combustion of DME/NH_3 mixtures is studied at different pressures (1, 10, 20, and 40 bar) under well-controlled laboratory-scale conditions. To accurately determine the molecular nitrogen formed during the reaction of the experiments, and therefore to perform nitrogen balances, argon is used as bath gas. The experimental setup, which has been used successfully in previous works [e.g. 4,8,9,28,40] is schematized in Fig. 1.

The reactant gases are fed from gas cylinders (providers: Air Liquide, Praxair, or Messer) and premixed before entering the quartz flow reactor (153.8 cm long, inner diameter of 0.6 cm), which is placed inside a 3-zone electrically heated oven, allowing an isothermal reaction zone (± 5 K) inside the tube of approximately 33 cm (± 3 cm). The temperature profiles along the reactor were determined using a type K thermocouple positioned in the space between the quartz tube and the steel shell used to keep the pressure constant. The temperature measurement was taken each 5 cm in the central zone and each 10 cm at both sides of the reactor. Fig. 2 shows, as an example, the temperature profiles obtained for the pressure of 20 bar, using a total gas flow rate of 1000 ml (STP)/min of argon. Profiles for the different pressures and temperatures were also determined.

In the present work, the effect of the main variables has been analyzed: oxygen excess ratio (reducing, λ = 0.7, stoichiometric, λ = 1, and oxidizing, λ = 3, conditions), pressure (1, 10, 20, and 40 bar), temperature (from 350 to 1225 K), and DME/NH_3 ratio of 0.05, and 0.3, which correspond to DME inlet nominal concentrations of 50 and 300 ppm, respectively, for a nominal NH_3 inlet concentration of 1000 ppm. The oxygen excess ratio (λ) is defined based on the NH_3 oxidation reaction to N_2 ($4NH_3 + 3O_2 \rightleftharpoons 2N_2 + 6H_2O$) (r1) and the DME oxidation reaction ($CH_3OCH_3 + 3O_2 \rightleftharpoons 2CO_2 + 3H_2O$) (r4), according to Eq. 1:

$$\lambda = \frac{[O_2]_{inlet}}{[O_2]_{stoichiometric}} \quad (1)$$

The total flow rate in all the experiments is 1000 ml (STP)/min and implies a temperature and pressure-dependent gas residence time in the isothermal reaction zone described in Eq. (2):

$$t_r\ (s) = \frac{V_{reactor}}{Q_{real}} \cdot \frac{T_{reference}}{P_{referece}} \cdot \frac{P_{real}}{T_{real}} = 231.6 \cdot \frac{P}{T} \quad (2)$$

where P is pressure in bar, T is the temperature in K, V is the volume in dm^3 and Q is the flow rate in dm^3/s.

Considering Eq. (2), the residence time in the 350 to 1225 K temperature range at atmospheric pressure goes from 0.2 to 0.8 s, and at 40 bar of pressure goes from 8.4 to 30.9 s.

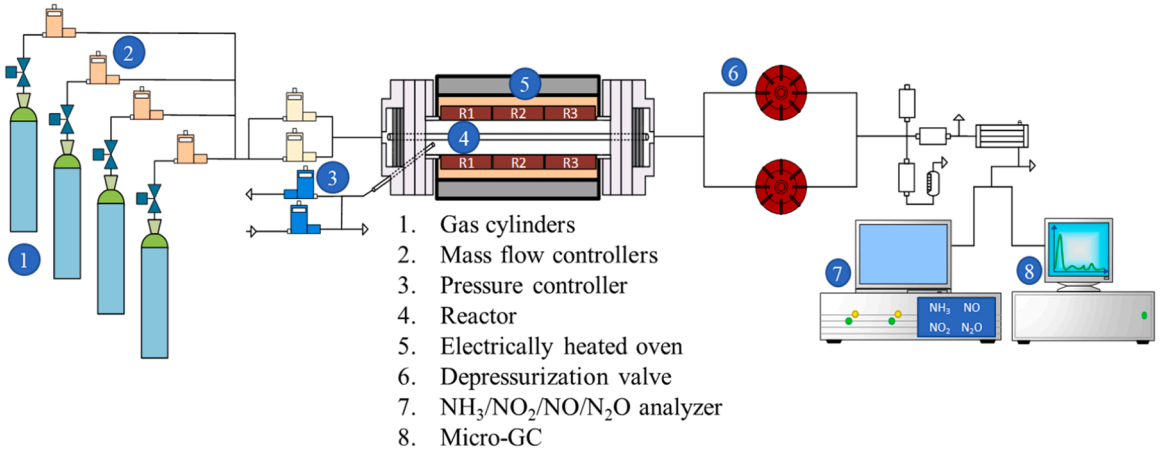

Fig. 1. Laboratory-scale high-pressure setup.

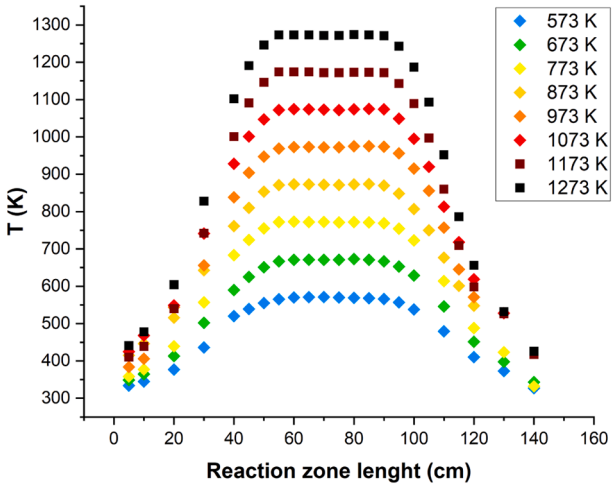

Fig. 2. Temperature profiles at 20 bar.

In the experiments, concentrations of NH_3, DME, NO, NO_2, N_2O, N_2, CO, CO_2, CH_4, O_2, H_2, and HCN are analyzed and quantified with a gas micro-chromatograph (Agilent Technologies), a NH_3/NO/NO_2/N_2O continuous analyzer (ABB, model: Advance Optima AO2020), a CO/CO_2 continuous analyzer (ABB, model: Advance Optima AO2000) and a Fourier-transform infrared (FTIR) spectroscopy analyzer (Protea, model: ProtIR 204M). The estimated uncertainty of the measurements is within ± 5 %, but not less than 5 ppm for the continuous analyzers and 10 ppm for the gas micro-chromatograph and FTIR determinations.

Table 1 summarizes the experimental initial conditions. The influence of pressure at different temperatures has been evaluated in the 1 to 40 bar range for λ = 1, and 3 (sets 1 - 8, and 10 - 17 in Table 1). For the highest pressure studied, 40 bar, we have also considered a fuel-rich stoichiometry of 0.7 (sets 9 in Table 1), as the experimental higher-pressure conditions allowed us to see the NH_3 reaction at comparatively lower temperatures.

Sets 8, 8(R1), 8(R2), 9, and 9(R), correspond, respectively, to repetition experiments. In this way, two or three results were obtained for each temperature. The reproducibility of the experiments is very good in all the temperature ranges considered, indicating the good performance of the experimental system and procedure. For the DME and NH_3 conversion data of experiments corresponding to conditions of sets 8, 8(R1), and 8(R2) in Table 1, and assuming that the experimental error does not depend on the temperature in the interval considered, the pooled standard deviation (the square root of the sum of squares of the error) has been calculated as an estimator of the experimental error associated

Table 1
Matrix of experimental conditions. All experiments are performed in the 350 - 1225 K temperature interval with a total flow rate of 1000 ml (STP)/min and using Ar as bath gas.

Set	DME (ppm)	NH_3 (ppm)	DME/NH_3	O_2 (ppm)	λ	P (bar)
1	48	1022	0.05	919	1.01	1
2	55	1012	0.05	905	0.98	10
3	50	1120	0.05	850	0.86	20
4	53	1070	0.05	921	0.96	40
5	50	997	0.05	2753	3.07	1
6	55	1013	0.05	2702	2.92	10
7	50	1006	0.05	2695	2.98	20
8	50	1054	0.05	2490	2.65	40
8(R1)	51	1047	0.05	2451	2.61	40
8(R2)	52	1152	0.05	2693	2.64	40
9	283	1029	0.3	1185	0.73	40
9R	298	976	0.3	1148	0.71	40
10	324	1132	0.3	1644	0.90	1
11	281	961	0.3	1632	1.04	10
12	247	1021	0.3	1466	0.97	20
13	287	1017	0.3	1543	0.95	40
14	295	963	0.3	4975	3.10	1
15	294	955	0.3	5007	3.13	10
16	288	969	0.3	5009	3.15	20
17	289	1011	0.3	5074	3.12	40

with the conversion of DME and NH_3 in the study area. The pooled standard deviation obtained is 0.0249 for DME and 0.0316 for NH_3. This pooled standard deviation enables the calculation of the error bars as the 95 % confidence intervals for the mean value associated with each repeated experiment, for the average DME and NH_3 conversion values of set 8, 8(R1), and 8(R2), as shown later, in Figs. 6 and Fig. 7 (see Section 4. Results and discussion).

Nitrogen and carbon atom balances were performed to evaluate the quality of the experiments and to determine if the measured species were the dominant ones under the studied conditions. The use of argon as a bath gas makes it possible to determine the N_2 concentration in the exhaust gases with precision. Fig. 3 shows, as an example, N and C atom balances at different pressures for DME/NH_3 = 0.3, and λ = 1 and 3 respectively, as a function of temperature.

The N balance is calculated considering the nitrogen atoms of the following species: NH_3, NO, NO_2, N_2O, HCN, and N_2. In certain conditions, some species are produced around the uncertainty of the equipment measurements, with values lower than 5 ppm in all cases (HCN, NO, and NO_2). Even so, those species have been considered for the mass balance. Fig. 3 also includes as a continuous line the N balance (in percentage) calculated with the model of the present work (see Section 3. Kinetic model development), considering the same species mentioned above. As can be noted, the calculated N balance is between 95 and 100

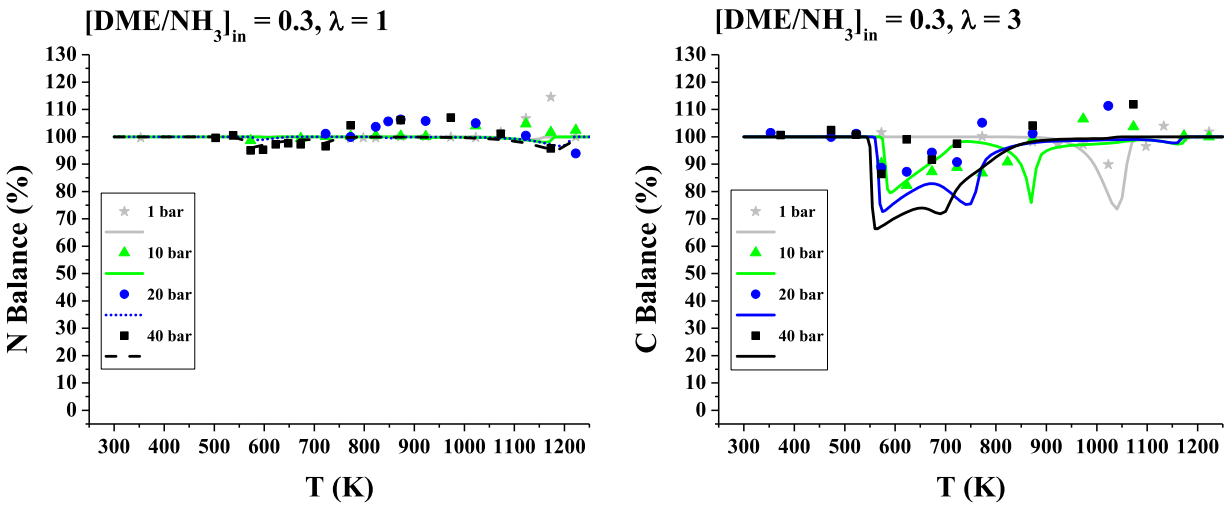

Fig. 3. Experimental and calculated N and C mass balances during the oxidation of DME/NH_3 mixtures, as a function of temperature, for different oxygen excess ratios and pressures. NH_3, NO, NO_2, N_2O, HCN, and N_2 species are included for N balance, and DME, CO, CO_2, CH_4, and HCN for C balance. Initial conditions correspond to sets 10 - 17 in Table 1.

%, while the experimental one closes between 90 and 110 % along the whole temperature range. This indicates that we are effectively quantifying all the main experimental N species and that the model reproduces reasonably well the experimental data.

However, for the C balance case, both the calculated and the experimental balance (considering in both cases CH_3OCH_3, CO, CO_2, CH_4, and HCN) is far from 100 % for certain temperatures. Calculations indicate that this is attributed to the presence of HOCHO, and CH_2O species for all pressures with a maximum peak of 158, and 43 ppm respectively for 40 bar and DME/NH_3 = 0.3, and in minor extent, to the presence of CH_3OCHO, $CH_3OCH_2O_2H$, HO_2CHO for high pressures, and C_2H_6, C_2H_4 for low pressure, with a maximum peak from 5 to 15 ppm. If we include these species with the calculated values in the experimental balance, it closes between 99.5 and 100 %. Those species may have been produced during the combustion of DME even though we do not measure them.

3. Kinetic model

The experimental results of the present work are analyzed and discussed using a gas-phase chemical kinetic mechanism developed in our group in previous work [9], which has been updated in the present work to capture the oxidation behavior of DME/NH_3 mixtures at high pressure. The main challenge was to consider the C-N interactions that might be present in the combustion of DME/NH_3 mixtures.

Calculations have been carried out using the plug-flow reactor (PFR) model of the Chemkin Pro suite [41], with the initial conditions for each experiment as listed in Table 1, and a "fix gas temperature" type problem, using the nominal reaction temperature at the flat temperature zone, since similar results were obtained with and without the measured temperature profiles.

The base mechanism used in the previous work of our group [9] is based on earlier work on nitrogen chemistry by Glarborg et al. [42], updated and modified with works of different authors (e.g. Stagni et al., Alzueta et al., Glarborg et al., Klippenstein et al., Burke et al., Marshall et al., [43–67]) to capture the main trends of the NH_3/H_2 and NH_3/CH_4 mixtures oxidation at high pressure.

In the present work, this base mechanism has been extended to include the conversion of DME, and C-N interactions happening at high pressure. For this purpose, the DME reaction subset from the work of Marrodán et al. [28] is included. That work captured very well the oxidation of DME and acetylene mixtures at high pressure, and the mechanism was validated under atmospheric pressure conditions [67] and modified to consider high-pressure conditions [28,56,67]. The compiled mechanism could predict the DME oxidation behavior accurately, but it presented several discrepancies for DME/NH_3 mixtures. That was because C-N interactions were needed to capture the DME/NH_3 mixture oxidation behavior under the high-pressure conditions of the present work and some DME reactions had to be updated. Some authors highlighted the importance of the C-N component reactions in the DME/NH_3 system [17,18]. The indications of these literature works are considered in the present work together with the findings of Stagni et al. [21] in relation to the DME reaction subset. The complete list of added reactions is included in Table S1 of supplementary material, and a discussion of the most relevant reactions involving the DME/NH_3 system (Table 2) is included as follows.

In relation to the most relevant reactions involving C-N interactions, we added reactions involving the interaction of carbon and nitrogen species from the works of Jiang et al. [19] (r6), Song et al. [68] (r7), Guan et al. [69] (r8 and r9), as well as other C-N interactions such as (r11) by Shi et al. [30].

Reaction $CH_3OCH_3 + OH \rightleftharpoons CH_3OCH_2 + H_2O$ (r5) has been extensively discussed in the literature. We consider updating the reaction rate constant with the one used by Marrodán et al. [28], which has a value of $k_5 = 6.71 \cdot 10^6 \cdot T^{2.00} \cdot e^{(629/RT)}$ $cm^3/(mol \cdot s)$ and was proposed by Tranter et al. [72] with a similar value to that proposed by Cook et al. [73] ($k_5 = 6.52 \cdot 10^6 \cdot T^{2.00} \cdot e^{(632/RT)}$ $cm^3/(mol \cdot s)$) who calculated the rate of the H-abstraction reaction of CH_3OCH_3 by OH in a shock tube from 0.61 to 11.65 bar in a 923-1423 K range using different transition state theories with tunneling corrections. Bänsch et al. [74] also evaluated the DME + OH interaction using a flow reactor from 5 to 21 bar in a 1349-1790 K range and did not observe pressure dependence of the rate constant. We implement the rate constant from Dai et al. [17] ($k_5 = 1,95 \cdot 10^7 \cdot T^{1.89} \cdot e^{(366/RT)}$ $cm^3/(mol \cdot s)$), which was proposed by Carr et al. [75] using a flow reactor system in a 0.03 to 0.3 bar pressure and 195-1423 K temperature ranges, and that is slightly slower compared to the original one in the mechanism.

Reaction $CH_3OCH_3 + NH_2 \rightleftharpoons CH_3OCH_2 + NH_3$ (r6) is pointed out as one of the most critical C-N interactions by Dai et al. [17], who calculated its rate constant value through quantum chemical calculations as $k_6 = 1.8 \cdot T^{3.61} \cdot e^{(-4353/RT)}$ $cm^3/(mol \cdot s)$. Later, Jiang et al. [19] refitted the reaction rate constant to a very similar value ($k_6 = 4.5 \cdot T^{3.61} \cdot e^{(-2353/RT)}$ $cm^3/(mol \cdot s)$), and this is the value that we have considered in the model of the present work.

For the DME + NO interaction, $CH_3OCH_3 + NO \rightleftharpoons CH_3OCH_2 + HNO$ (r7), there is an experimental and theoretical work by McKenney et al.

Table 2
Relevant selected reactions in the DME/NH_3 reaction system. Kinetic parameters of the modified Arrhenius equation for the selected reactions. Units in: s^{-1}, cm^3, cal, mol.

N°	Reaction	A	n	E_a	Ref
r5	$CH_3OCH_3 + OH \rightleftharpoons CH_3OCH_2 + H_2O$	$2.00{\cdot}10^{7}$	1.89	-365	[17]
r6	$CH_3OCH_3 + NH_2 \rightleftharpoons CH_3OCH_2 + NH_3$	4.5	3.61	2353	[19]
r7	$CH_3OCH_3 + NO \rightleftharpoons CH_3OCH_2 + HNO$	$5.24{\cdot}10^{-1}$	4.227	40782	[68]
r8	$CH_3OCH_3 + NO_2 \rightleftharpoons CH_3OCH_2 + HNO_2$	$6.5{\cdot}10^{2}$	3.00	23176	[69]
r9	$CH_3OCH_3 + NO_2 \rightleftharpoons CH_3OCH_2 + HONO$	$5.8{\cdot}10^{1}$	3.50	23755	[69]
r10	$CH_3OCH_2 \rightleftharpoons CH_2O + CH_3$	$8.03{\cdot}10^{12}$	-0.440	26491	[25]
	PLOG (0.01)	$7.49{\cdot}10^{23}$	-4.515	25236	
	PLOG (0.1)	$6.92{\cdot}10^{28}$	-5.727	27495	
	PLOG (1)	$4.23{\cdot}10^{29}$	-5.610	28898	
	PLOG (10)	$6.61{\cdot}10^{27}$	-4.707	29735	
	PLOG (100)	$2.66{\cdot}10^{29}$	-4.936	31786	
r11	$CH_2O + NH_2 \rightleftharpoons HCO + NH_3$	$2.27{\cdot}10^{3}$	2.933	5471	[30]
	duplicate reaction	4.51	3.812	1483	
r12	$CH_2OCH_2O_2H \rightleftharpoons CH_2O + CH_2O + OH$	$8.12{\cdot}10^{37}$	-9.15	21314	[70]
	PLOG (0.987)	$8.12{\cdot}10^{37}$	-9.15	21314	
	PLOG (2.961)	$5.4{\cdot}10^{43}$	-10.8	23815	
	PLOG (6.168)	$1.6{\cdot}10^{44}$	-10.83	24408	
	PLOG (12.337)	$9.4{\cdot}10^{41}$	-10.04	24043	
	PLOG (24.673)	$9.5{\cdot}10^{37}$	-8.71	23034	
	PLOG (49.346)	$3.4{\cdot}10^{33}$	-7.24	21851	
	PLOG (98.692)	$8.9{\cdot}10^{29}$	-6.05	20964	
r13	$CH_2OCH_2O_2H + O_2 \rightleftharpoons O_2CH_2OCH_2O_2H$	$1.1{\cdot}10^{22}$	-3.30	3389	[25]
	PLOG (0.001)	$9.4{\cdot}10^{12}$	-1.68	-4998	
	PLOG (0.01)	$8.2{\cdot}10^{16}$	-2.5	-2753	
	PLOG (1)	$1.1{\cdot}10^{22}$	-3.3	3389	
	PLOG (2)	$3.5{\cdot}10^{20}$	-2.79	3131	
	PLOG (10)	$2.9{\cdot}10^{16}$	-1.48	1873	
	PLOG (20)	$8.6{\cdot}10^{14}$	-1.01	1312	
	PLOG (50)	$2.7{\cdot}10^{13}$	-0.54	727	
	PLOG (100)	$4.9{\cdot}10^{12}$	-0.32	428	
r14	$HO_2CH_2OCHO \rightleftharpoons OCH_2OCHO + OH$	$5.0{\cdot}10^{16}$	2.13	27500	[17]
r15	$NH_3 + OH \rightleftharpoons NH_2 + H_2O$	$4.5{\cdot}10^{10}$	0.56	1451	[71]
r16	$H_2NO + O_2 \rightleftharpoons HNO + HO_2$	$2.3{\cdot}10^{2}$	2.994	18900	[5]
r17	$H_2NO + NH_2 \rightleftharpoons HNO + NH_3$	$9.48{\cdot}10^{12}$	-0.081	-1643	[55]
r18	$NH_2 + NO \rightleftharpoons NNH + OH$	$4.3{\cdot}10^{10}$	0.294	-866	[53]

[76] that reported a value of $1.00{\cdot}10^{14}{\cdot}e^{(-43400/RT)}$ $cm^3/(mol{\cdot}s)$ for k_7 and a recent theoretical value, obtained through quantum chemical calculations in the 200–3000 K temperature range, proposed by Song et al. [68] ($k_7 = 5.24{\cdot}10^{-1}{\cdot}T^{4.23}{\cdot}e^{(-40782/RT)}$ $cm^3/(mol{\cdot}s)$), which we have adopted in the updated mechanism.

In the case of the DME + NO_2 interaction: $CH_3OCH_3 + NO_2 \rightleftharpoons CH_3OCH_2 + HNO_2$ (r8) and $CH_3OCH_3 + NO_2 \rightleftharpoons CH_3OCH_2 + HONO$ (r9), there are several chemical kinetic reaction rates proposed in the literature [29,69,77–79] with values that differ from each other. Dagaut et al. [77] proposed reaction rates for the DME + NO_2 consumption ($k_9 = 9.00{\cdot}10^{12}{\cdot}e^{(-17600/RT)}$ $cm^3/(mol{\cdot}s)$) based on DME oxidation results in a jet-stirred reactor in a narrow temperature range (550–800 K), which exhibited significant uncertainty according to Guan [69]. Ye et al. [78] studied the NO_2 effect in the ignition characteristic of DME and calculated the reaction rate for reactions as (r8) ($k_8 = 2.41{\cdot}10^{3}{\cdot}T^{2.90}{\cdot}e^{(-27470/RT)}$ $cm^3/(mol{\cdot}s)$) and (r9) ($k_9 = 1.45{\cdot}10^{2}{\cdot}T^{3.32}{\cdot}e^{(-20035/RT)}$ $cm^3/(mol{\cdot}s)$) by analogy to the CH_3OH/NO_2 reaction system. The H-abstraction reactions by NO_2 from DME determined by Shang et al. [79] ($k_8 = 4.5{\cdot}10^{9}{\cdot}T^{1.01}{\cdot}e^{(-26816/RT)}$ $cm^3/(mol{\cdot}s)$) and ($k_9 = 5.19{\cdot}10^{4}{\cdot}T^{2.56}{\cdot}e^{(-23700/RT)}$ $cm^3/(mol{\cdot}s)$), through quantum chemical calculations from 500-2000 K, show significant discrepancies with the rate constants proposed by Ye et al. [78]. More recently, Pelucchi et al. [29] performed a theoretical evaluation of DME + NO_2 and adopted the reaction rate constant of Dagaut et al. [77] for reaction (r8) proposing the same reaction rate for reaction (r9). They consider that some discrepancies still exist with the experimental findings and recommended a further re-evaluation. In our work, we adopt the rate constant proposed by Guan et al. [69] ($k_8 = 6.5{\cdot}10^{2}{\cdot}T^{3.00}{\cdot}e^{(-23176/RT)}$ $cm^3/(mol{\cdot}s)$ and $k_9 = 5.8{\cdot}10^{1}{\cdot}T^{3.50}{\cdot}e^{(-23755/RT)}$ $cm^3/(mol{\cdot}s)$).

Regarding the $CH_3OCH_2 \rightleftharpoons CH_2O + CH_3$ (r10) reaction, Dai et al. [17] propose a reaction rate constant fitted from the results of Gao et al. [80] ($k_{10} = 3.4{\cdot}10^{13}{\cdot}T^{-0.71}{\cdot}e^{(-21037/RT)}$ s^{-1})), with pressure dependence, slightly similar to that proposed by Burke et al. [25] ($k_{10} = 7.49{\cdot}10^{29}{\cdot}T^{-5.61}e^{(-28898/RT)}$ s^{-1}) and to Sehested et al. [81] ($k_{10} = 1.60{\cdot}10^{13}{\cdot}e^{(-25436/RT)}$ s^{-1}) which did not include any pressure dependence. Taking into consideration the experimental and modeling ignition work for delay time measurement at 7 to 41 bar and 600-1600 K by Burke et al. [25], we have included a pressure dependence as they point out, and selected their proposed reaction rate constant because of the great fit with our experimental system and the adaptation of that constant for several pressures.

In the case of the reaction $CH_2O + NH_2 \rightleftharpoons HCO + NH_3$ (r11), the theoretical determination of Li et al. [82] at 298K was adopted in the Dai et al. model [17]. Recently, Zhu et al. [22] divided the Li et al. [82] constant by 20, and their calculations showed a good performance in the low-temperature region. Shi et al. [30] proposed a new value for the rate constant calculated by the Rice-Ramspenger-Kassel-Marcus (RRKM)/master-equation analysis at 373 K for pressures up to 5 bar ($k_{11} = 2.27{\cdot}10^{3}{\cdot}T^{-2.933}{\cdot}e^{(-5471/RT)}$ s^{-1}), which has been adopted in the present work. This reaction is relevant because CH_2O is an important intermediate of the DME oxidation and the H-abstraction from CH_2O by NH_2 is significant under any temperature range [30].

For reactions $CH_2OCH_2O_2H \rightleftharpoons CH_2O + CH_2O + OH$ (r12) and $CH_2OCH_2O_2H + O_2 \rightleftharpoons O_2CH_2OCH_2O_2H$ (r13), we updated the reaction rate constants adopted by Marrodán et al. [28] with the rates proposed by Eskola et al. [70] ($k_{12} = 8.1{\cdot}10^{37}{\cdot}T^{-9.15}{\cdot}e^{(-22243/RT)}$ s^{-1}) and Burke et al. [25] ($k_{13} = 1.10{\cdot}10^{22}{\cdot}T^{-3.30}{\cdot}e^{(-3389/RT)}$ $cm^3/(mol{\cdot}s)$) respectively, as they considered the pressure dependence.

The reaction $HO_2CH_2OCHO \rightleftharpoons OCH_2OCHO + OH$ (r14), has been added in the present work to the mechanism, with the rate constant ($k_{14} = 5.0{\cdot}10^{6}{\cdot}e^{(-43000/RT)}$ s^{-1}) following the work of Dai et al. [17] mechanism.

For reaction $NH_3 + OH \rightleftharpoons NH_2 + H_2O$ (r15), we considered the recent determination of Stagni et al. [83] ($k_{15} = 1.56{\cdot}10^{5}{\cdot}T^{2.37}{\cdot}e^{(-119/RT)}$ $cm^3/(mol{\cdot}s)$) by ab initio transition state theory-based master equation approach, but we adopted the constant proposed by Samu et al. [71] ($k_{15} = 4.5{\cdot}10^{10}{\cdot}T^{0.56}{\cdot}e^{(-1451/RT)}$ $cm^3/(mol{\cdot}s)$), who optimized the reaction rate constant proposed by Diau et al. [84] through indirect methods based on literature data.

H_2NO has been mentioned to be an important intermediate species during NH_3 oxidation [51,55,85]. In particular, under the conditions of the present work, $H_2NO + O_2 \rightleftharpoons HNO + HO_2$ (r16) is crucial for NH_3 consumption. We have selected the rate proposed by Song et al. [5] ($k_{16} = 2.3{\cdot}10^{2}{\cdot}T^{2.99}{\cdot}e^{(-18900/RT)}$ $cm^3/(mol{\cdot}s)$) because they consider high-pressure conditions. For the $H_2NO + NH_2 \rightleftharpoons HNO + NH_3$ (r17) and $NH_2 + NO \rightleftharpoons NNH + OH$ (r18) reactions, we have maintained, respectively, the rates taken from the work of Stagni et al. [55] ($k_{17} = 9.48{\cdot}10^{12}{\cdot}T^{-0.08}{\cdot}e^{(1643/RT)}$ $cm^3/(mol{\cdot}s)$) and the work of Glarborg et al. [53] ($k_{18} = 4.30{\cdot}10^{10}{\cdot}T^{0.294}{\cdot}e^{(866/RT)}$ $cm^3/(mol{\cdot}s)$).

The H-abstraction reaction of CH_3OCH_3 and NH_3 by reaction with OH ($CH_3OCH_3 + OH \rightleftharpoons CH_3OCH_2 + H_2O$ (r5) and $NH_3 + OH \rightleftharpoons NH_2 + H_2O$ (r15), respectively) show a considerable sensitivity in the conversion of DME and NH_3. These reactions are widely discussed in the literature and to illustrate the sensitivity level of DME and NH_3 conversion, simulations have been performed considering the kinetic constants of Table 3 and 4, for reactions (r5) and (r15) respectively.

Fig. 4 shows the effect of varying $CH_3OCH_3 + OH \rightleftharpoons CH_3OCH_2 + H_2O$ (r5) and Fig. 5 the effect of varying $NH_3 + OH \rightleftharpoons NH_2 + H_2O$ (r15) on the conversion of both DME and NH_3 in the combustion of DME/NH_3 mixtures, at 10 and 40 bar of pressure for DME/NH_3 = 0.3, $\lambda = 3$, as an

Table 3
Selected kinetic parameters of the modified Arrhenius equation for reaction $CH_3OCH_3 + OH \rightleftharpoons CH_3OCH_2 + H_2O$ (r5). Units in: s^{-1}, cm^3, cal, mol.

A	n	Ea	Source
$6.71{\cdot}10^6$	2.00	-630	Tranter et al. [72]
$6.32{\cdot}10^6$	2.00	-652	Cook et al. [73]
$5.09{\cdot}10^6$	2.07	-521	Bansch et al. [74]
$2.00{\cdot}10^7$	1.89	-365	Dai et al. [17]
$1.95{\cdot}10^7$	1.89	-366	Car et al. [75]
$2.19{\cdot}10^7$	1.91	-374	Stagni et al. [21]

Table 4
Selected kinetic parameters of the modified Arrhenius equation for reaction $NH_3 + OH \rightleftharpoons NH_2 + H_2O$ (r15). Units in: s^{-1}, cm^3, cal, mol.

A	n	Ea	Source
$2.00{\cdot}10^6$	2.04	566	Salimian et al. [86]
$1.56{\cdot}10^5$	2.37	119	Stagni et al. [83]
$4.50{\cdot}10^{10}$	0.56	1451	Samu et al. [71]

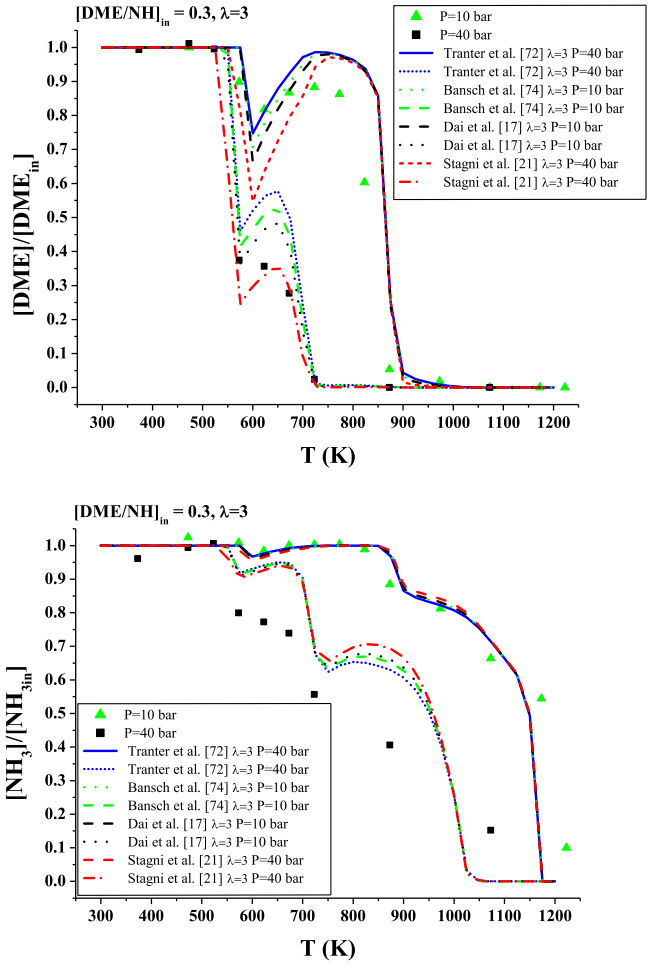

Fig. 4. DME and NH_3 conversion as a function of temperature for different pressures (10 and 40 bar) varying $CH_3OCH_3 + OH \rightleftharpoons CH_3OCH_2 + H_2O$ (r5). Sets 15 and 17 in Table 1. $DME/NH_3 = 0.3$, $\lambda = 3$. Ar as bath gas. Symbols represent experimental data and lines for calculations.

example. For the comparison of reaction (r5), the reaction rate constants from Samu et al. [71] have been selected for reaction (r15). On the other hand, when the reaction (r15) is varied, the reaction rate constants from Dai et al. [17] have been chosen for the reaction (r5). Some rate constants are not shown in Figs. 4 and Fig. 5 due to the similarity between them. As can be seen, DME and NH_3 conversion trends are quite

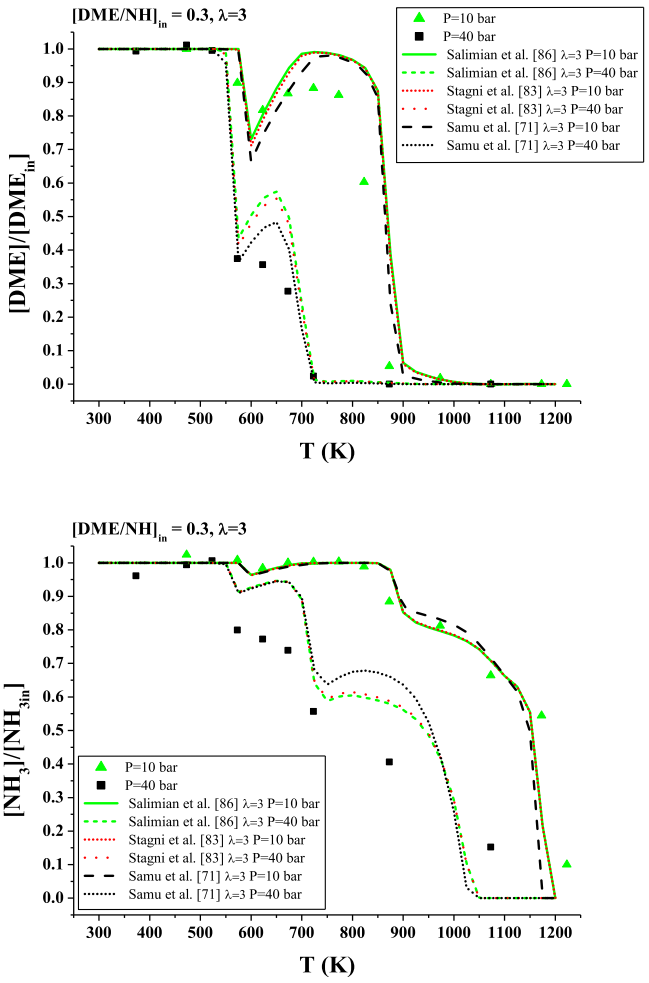

Fig. 5. DME and NH_3 conversion as a function of temperature for different pressures (10 and 40 bar) varying $NH_3 + OH \rightleftharpoons NH_2 + H_2O$ (r15). Sets 15 and 17 in Table 1. $DME/NH_3 = 0.3$, $\lambda = 3$. Ar as bath gas. Symbols represent experimental data and lines for calculations.

remarkable, with the differences more accentuated for higher pressure and oxygen availability (see Figure S1 and S2 of supplementary material).

As can be seen, and will be discussed later in more detail, both DME and NH_3 show a negative temperature coefficient (NTC) behavior, also reported by other authors [e.g. 19-24, 29]. DME shows two different combustion stages, one at low temperature (450–650 K), and another at high-temperature T > 700 K, and between them, the DME combustion shows a transition zone from 650–700 K, which is in line with other authors [e.g. 29]. Independently on the pressure rate constant considered for reactions (r5) and (r15), reported in Tables 3 and 4, the mechanism is able to capture the DME and NH_3 conversion trends. However, differences in the transition zone appear as a function of the considered rate constant value. In addition, these differences are more accentuated for higher pressure and oxygen availability. Important reactions for DME consumption are $CH_2OCH_2O_2H + O_2 \rightleftharpoons O_2CH_2OCH_2O_2H$ (r13) and $HO_2CH_2OCHO \rightleftharpoons OCH_2OCHO + OH$ (r14), which are responsible for NTC behavior in the transition zone.

The updated mechanism of the present work has been validated with experimental results obtained in the present study (results shown in Figures of Section 4. Results and discussion) and with experimental data from the literature (results shown in Figures S3 and S4 of the supplementary material). The performance of the model is very good for both, our experimental and literature results, for the conversion of DME/NH_3 mixtures under a variety of conditions (in particular, flow reactor data

and ignition delay times).

4. Results and discussion

A combined experimental and modeling study addressing the oxidation of DME/NH_3 mixtures with different O_2 concentrations using Ar as bath gas has been performed in a quartz flow reactor, operating from atmospheric pressure to high pressure (1, 10, 20 and 40 bar), in the 350-1225 K temperature range and for fuel rich to fuel lean conditions (λ = 0.7, 1 and 3). The specific experimental conditions are summarized in Table 1. In the figures, symbols denote experimental results and line model calculations.

Fig. 6 shows the NH_3 conversion as a function of temperature for different pressures (from 1 to 40 bar), different DME/NH_3 (0.05 and 0.3), and oxygen excess ratios (λ = 1 and 3). As can be seen, the reproducibility of the experiments is very good in all the temperature ranges considered.

The reaction onset temperature of NH_3 oxidation and its concentration at a given temperature show a pressure dependence. In both cases, they are markedly decreased with increasing pressure for all pressures studied. This behavior was also observed with pure NH_3 oxidation at high pressure [4,5], as well as for its mixtures with CH_4 [9] and H_2 [8,33] at high pressure. The pressure effect on the NH_3 conversion depends directly on the DME/NH_3 ratio, keeping similar to the rest of the conditions. This is in line with the findings of other authors [17] who concluded that the ignition curve as a function of temperature is shifted to 150 and 250 K less for DME/NH_3 = 0.02 and 0.06 respectively.

Comparing the effect of DME with that of H_2 [8] and CH_4 [9] on NH_3 conversion, for $\lambda = 3$, and 40 bar conditions, the NH_3 reaction onset in its mixtures with DME (DME/NH_3 = 0.3) starts at 550 K; this is 250, 300, and 600 K less than for the combustion of the NH_3/H_2 mixture (H_2/NH_3 = 0.5 and 1) [8], the CH_4/NH_3 mixture (CH_4/NH_3 = 0.5 and 1) [9] and pure NH_3 [4] combustion, respectively, under similar experimental conditions but with a lower DME/NH_3 ratio (i.e. 0.05). This is an indication of the potential of DME as an additive in NH_3 combustion.

Fig. 7 shows the DME conversion as a function of temperature for different pressures (from 1 to 40 bar), different DME/NH_3 ratios (0.05, and 0.3), and oxygen excess ratios ($\lambda = 1$ and 3). As can be seen in Fig. 7, the model can reproduce well the experimental data.

As for NH_3, the DME reaction onset temperature depends strongly on pressure. The temperature at which DME is fully consumed also decreases noticeably with pressure, especially in the case of DME = 300 ppm.

It can be noted that the beginning and the end of the transition zone of both NH_3 and DME take place at the same temperature range for DME/NH_3 = 0.3. In addition, the ammonia conversion occurs at a lower temperature compared to the net NH_3 combustion [4], this makes clear the effect of DME on NH_3 consumption.

Fig. 8 shows, the NH_3 conversion profiles varying the oxygen excess ratio (λ = 0.7, 1, and 3) at 40 bar for DME/NH_3 = 0.3, as an example. Both experimental and modeling results show a noticeable effect of oxygen availability between stoichiometric and oxidizing conditions, while there are no major differences in NH_3 consumption between stoichiometric and reducing conditions. On the contrary, for the conversion of net NH_3 [4] and its mixtures with H_2 [8] and CH_4 [9], the reaction onset temperature hardly varies for different oxygen ratios. However, it is remarkable that under the conditions of Fig. 8, full NH_3 conversion is reached at lower temperatures compared to the mixtures mentioned above and neat NH_3.

To compare the effects of the mixture composition, Fig. 9 shows the NH_3 conversion as a function of temperature keeping a similar pressure and stoichiometry for two different DME nominal initial concentrations (50 and 300 ppm) and a given nominal initial NH_3 concentration (1000 ppm). The addition of DME results in a decrease in the NH_3 reaction onset temperature. Also, a more remarkable ammonia-NTC behavior appears as the DME/NH_3 ratio increases. The DME addition to the combustion mixture produces a higher concentration of OH radicals

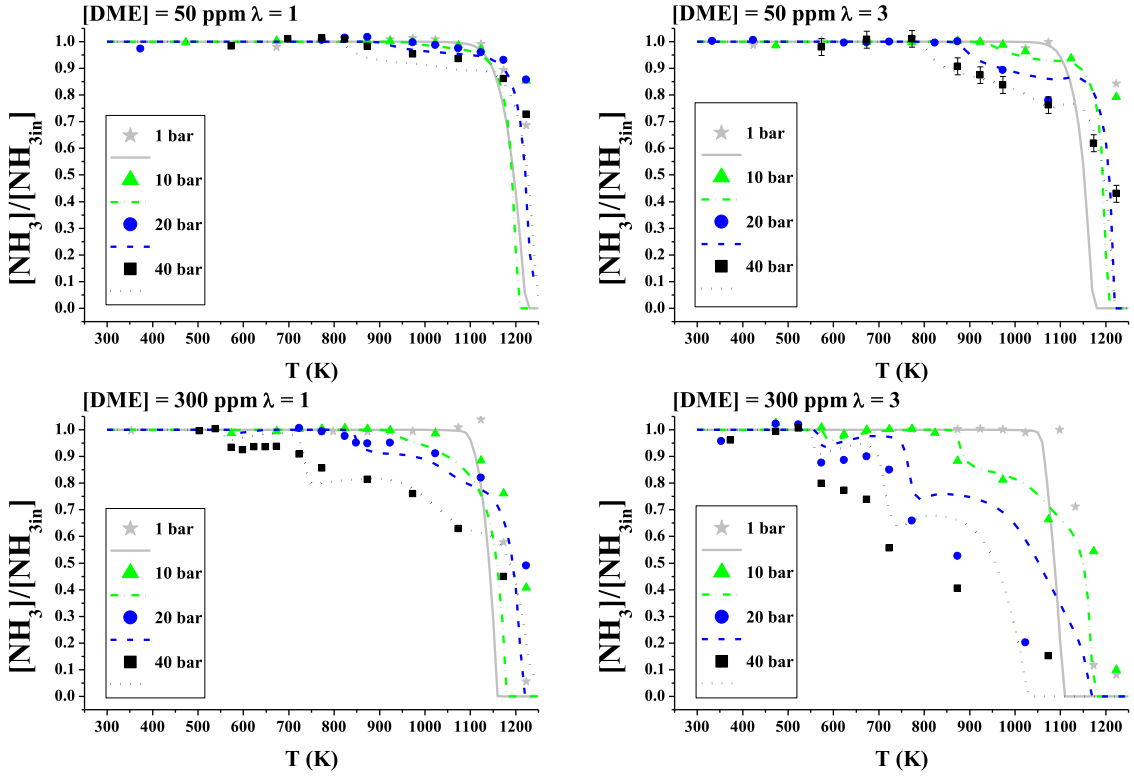

Fig. 6. NH_3 conversion as a function of temperature for different pressures (1 - 40 bar). Sets 1-8 and 10-17 in Table 1. DME/NH_3 = 0.05 and 0.3, [NH_3] = 1000 ppm, λ = 1 and 3.

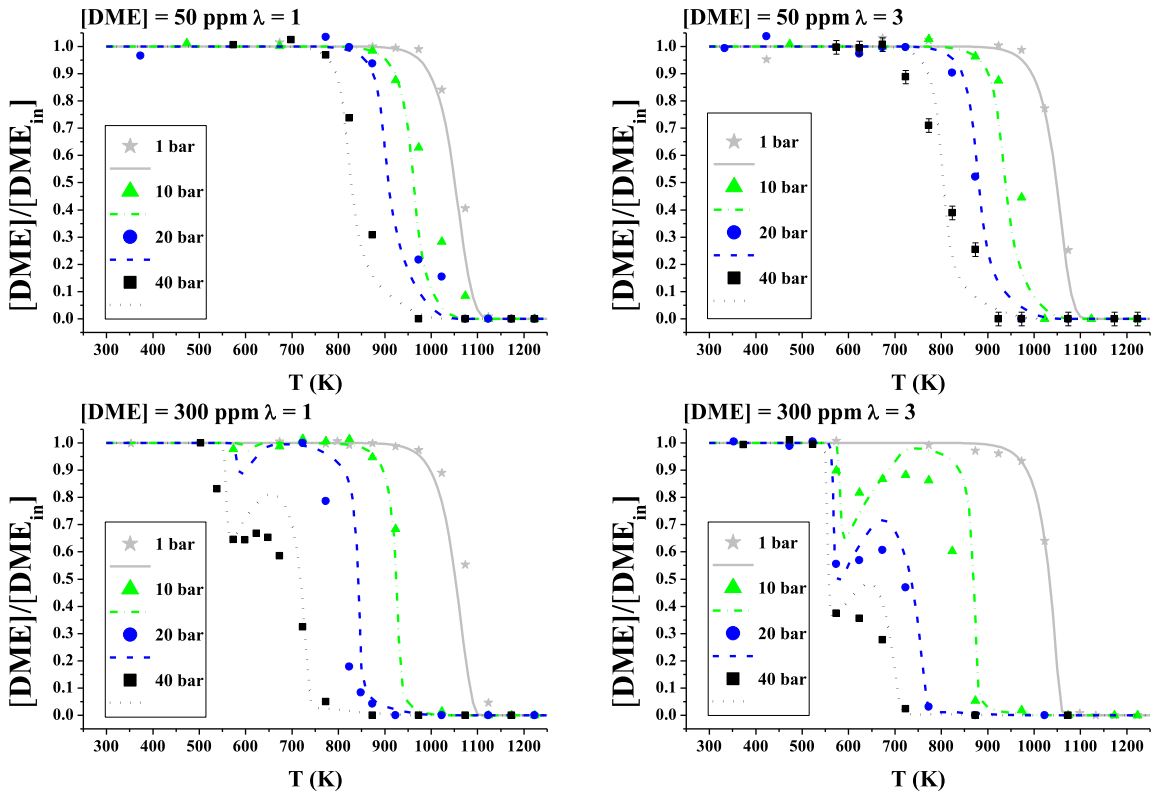

Fig. 7. DME conversion as a function of temperature for different pressures (1 - 40 bar). Sets 1-8 and 10-17 in Table 1. DME/NH_3 = 0.05 and 0.3, [NH_3] = 1000 ppm, λ = 1 and 3.

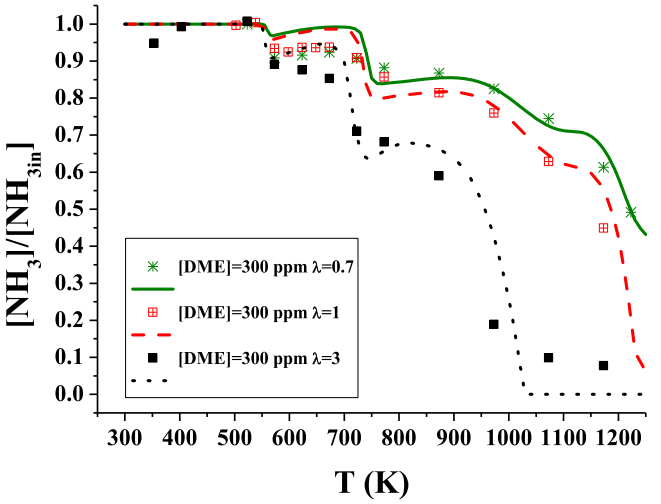

Fig. 8. NH_3 conversion as a function of temperature at 40 bar for different oxygen stoichiometric (λ = 0.7, 1 and 3). Sets 9, 13 and 17 in Table 1. DME/NH_3 = 0.3, [NH_3] = 1000 ppm.

once the transition zone has been overcome by the temperature effect (as discussed below), resulting in a higher NH_3 consumption in the presence of DME.

To get some insight into the reaction pathway through which the DME/NH_3 combustion proceeds at high pressure, we have made reaction pathway analyses for the different temperatures considered. Since the main trends of species conversion are well captured by the model, this is an indication that the main reaction pathways can be feasible. Fig. 10 shows the reaction path diagram for NH_3 consumption for 3 different combustion situations: the low-temperature (LT) combustion regime (555 K), during the transition zone (NTC) (610 K), and the high-temperature (HT) combustion regime (725 K). It can be noted that the NH_3 combustion presents 3 different reaction pathways. The difference between the low-temperature (LT) and transition zone (NTC) is the appearance of the NH_3 production reactions. In the high-temperature (HT) combustion regime, a new reaction pathway appears involving interactions between NH_2 and NO_2 that produce H_2NO and NO (r19). As can be seen in Fig. 10, the main NH_3 consumption reaction is H-abstraction via OH (r15) as well as was observed for pure NH_3 [4] combustion and in its mixtures with H_2 [8] and CH_4 [9]. NH_3 production occurs through reactions of NH_2 with CH_2O (r11), tHNNH (r20), HO_2 (r21), H_2O_2, (r22), and N_2H_4 (r23). These NH_3 production reactions only appear in the transition zone to the high-temperature regime.

$$CH_2O + NH_2 \rightleftharpoons HCO + NH_3 \quad \text{(r11)}$$

$$NH_3 + OH \rightleftharpoons NH_2 + H_2O \quad \text{(r15)}$$

$$NH_2 + NO_2 \rightleftharpoons H_2NO + NO \quad \text{(r19)}$$

$$tHNNH + NH_2 \rightleftharpoons NH_3 + NNH \quad \text{(r20)}$$

$$NH_2 + HO_2 \rightleftharpoons NH_3 + O_2 \quad \text{(r21)}$$

$$NH_2 + H_2O_2 \rightleftharpoons NH_3 + HO_2 \quad \text{(r22)}$$

$$N_2H_4 + NH_2 \rightleftharpoons N_2H_3 + NH_3 \quad \text{(r23)}$$

As seen in Fig. 10, the $NH_3 \rightarrow NH_2 \rightarrow N_2H_4 \rightarrow tHNNH \rightarrow NNH \rightarrow N_2$ and $NH_3 \rightarrow N_2O \rightarrow N_2$ are the two major NH_3 consumption channels. In the high-temperature region, $NH_3 \rightarrow NH_2 \rightarrow H_2NO \rightarrow HONO/HNO \rightarrow NO \rightarrow NO_2$ also shows up as a reaction pathway. The last one is the most significant pathway under atmospheric pressure conditions (Figure S5 of the supplementary material). Another difference at atmospheric pressure is the hydrogen abstraction reaction of DME by NH_2 radicals (r6) and the relevance of reaction (r24) producing CH_3NH_2 (Figures S5 and S6 of the supplementary material).

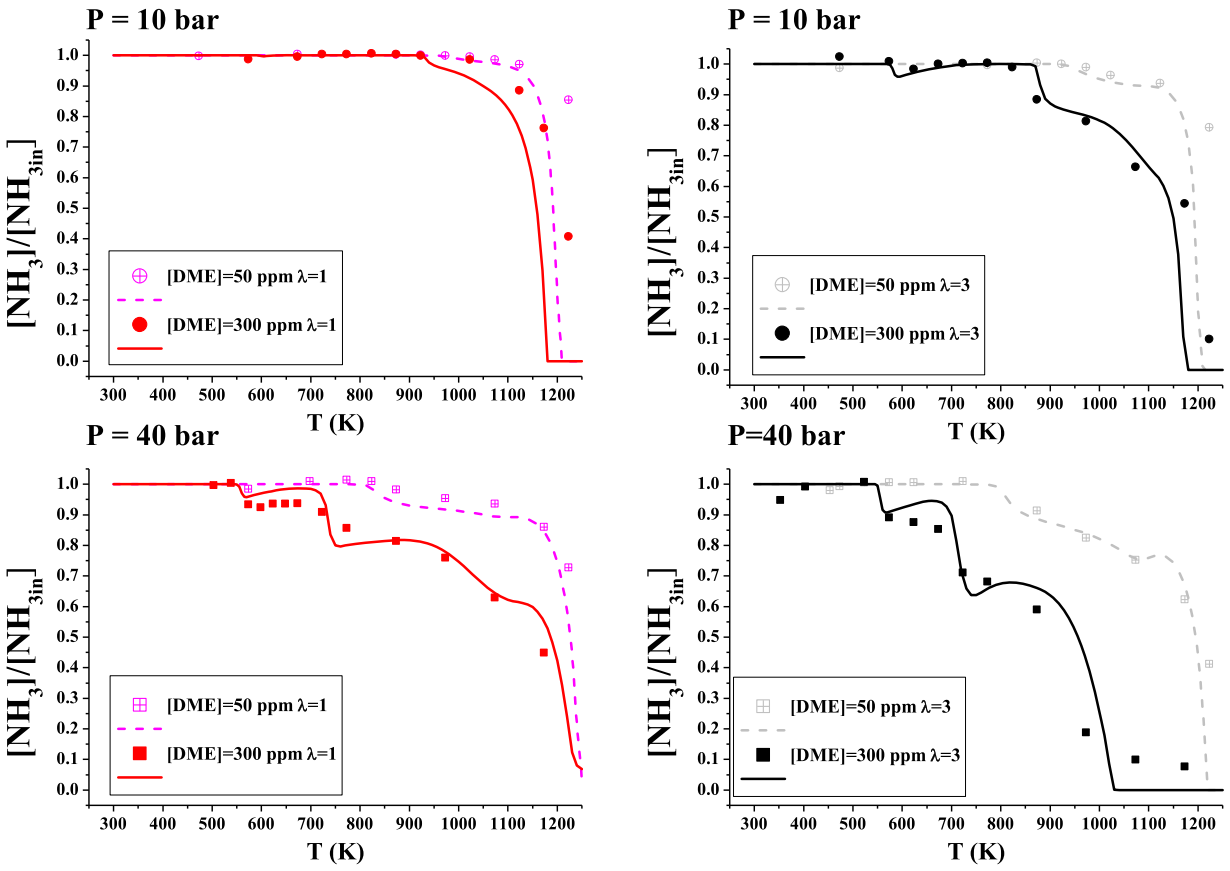

Fig. 9. NH_3 conversion as a function of temperature at 10 and 40 bar for different oxygen stoichiometric ($\lambda = 1$ and 3). Sets 2, 4, 6, 8, 11, 13, 15 and 17 in Table 1. $DME/NH_3 = 0.05$ and 0.3, $[NH_3] = 1000$ ppm.

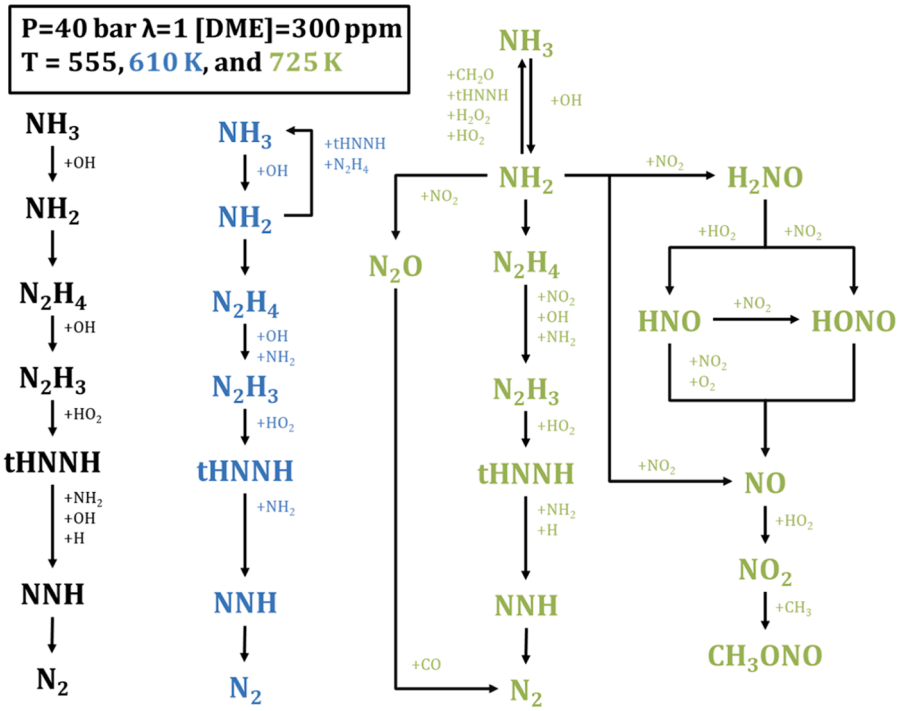

Fig. 10. Reaction path diagram for consumption of NH_3 at $DME/NH_3 = 0.3$, stoichiometric ($\lambda = 1$) conditions at 40 bar for T = 555, 610 and 725 K. Sets 13 in Table 1. The reaction path for CH_3ONO is shown in Fig. 11.

$$CH_3OCH_3 + NH_2 \rightleftharpoons CH_3OCH_2 + NH_3 \quad (r6)$$

$$CH_3 + NH_2 \rightleftharpoons CH_3NH_2 \quad (r24)$$

Concerning NO_2, its production occurs through the reaction of NO with HO_2 (r25), which is known to be the dominant formation reaction under high-pressure conditions. NO_2 is involved in a multitude of reactions and is consumed instantly, by reaction with NH_2, H_2NO, HNO, OH, H, N_2H_4, CH_2O, and HCO among others. However, its reaction with CH_3 to form CH_3ONO (r26) and with NH_2 to form H_2NO and NO (r19) are the most important ones. Thus, no appreciable quantities of NO_2 species are found at the reactor outlet. Also, NH_4NO_3 may be potentially be formed [4].

$$NO + HO_2 \rightleftharpoons NO_2 + OH \quad (r25)$$

$$CH_3 + NO_2 (+M) \rightleftharpoons CH_3ONO (+M) \quad (r26)$$

The main production of NO occurs through the reaction of NO_2 with NH_2 and HNO (r19 and r27), and the decomposition of both CH_3ONO and HONO (-r28 and -r29), mainly in the high-temperature region because the CH_3ONO and HONO species appear at temperatures above the transition zone. The CH_3ONO production comes from C-N interactions, as was observed for CH_4/NH_3 mixtures [9]. Experimentally, NO is only produced for the DME/NH_3 ratio of 0.3 and atmospheric pressure, reaching 40 and 140 ppm at the highest temperature considered, for $\lambda = 1$ and 3 respectively (Figure S7 in supplementary material). This points to the benefit of working at high pressure to limit the production NO. The NO consumption occurs through its reaction with HO_2 to form NO_2 (r25), as mentioned before, and with NH_2 to form N_2 (r30).

$$HNO + NO_2 \rightleftharpoons HONO + NO \quad (r27)$$

$$CH_3O + NO (+M) \rightleftharpoons CH_3ONO (+M) \quad (r28)$$

$$OH + NO \rightleftharpoons HONO \quad (r29)$$

$$NH_2 + NO \rightleftharpoons N_2 + H_2O \quad (r30)$$

For $DME/NH_3 = 0.3$ at a given temperature (Figure S7), the NO concentration increases for oxidizing conditions, because the oxygen availability favors the NO production during DME/NH_3 combustion, as was also observed for other C-containing fuel mixtures like CH_3OH/NH_3 [e.g. 11]. For $DME/NH_3 = 0.05$, no appreciable amount of NO has been found in the exhaust gases. As seen in Figure S7 model reproduces well the experimental observations.

Fig. 11 shows the reaction path diagram for DME consumption at 555, 610, and 725 K. The conversion of DME presents two different reaction pathways: the one at the low-temperature oxidation regime and the transition zone between low and high-temperature regimes, and then the second one at the high-temperature oxidation regime, in which the formation of CH_3 radicals and their subsequent transformation into CH_3ONO (r26) to finally produce NO (-r28) represents the main difference.

As can be seen in Fig. 11, the main DME consumption reaction is its H-abstraction by OH (r5) to generate CH_3OCH_2. The CH_3OCH_2 formed is quickly oxidized by O_2 into $CH_3OCH_2O_2$ (r31), which could be one of the reasons why the NTC behavior is more remarkable under oxidizing conditions. The $CH_3OCH_2O_2$ formed suffers recombination to $CH_2OCH_2O_2H$ radicals (r32), which in turn they have two consumption paths: decomposition into CH_2O and OH (r12) and oxidation to form $O_2CH_2OCH_2O_2H$ (r13).

$$CH_2OCH_2O_2H \rightleftharpoons CH_2O + CH_2O + OH \quad (r12)$$

$$CH_2OCH_2O_2H + O_2 \rightleftharpoons O_2CH_2OCH_2O_2H \quad (r13)$$

$$CH_3OCH_2 + O_2 \rightleftharpoons CH_3OCH_2O_2 \quad (r31)$$

$$CH_3OCH_2O_2 \rightleftharpoons CH_2OCH_2O_2H \quad (r32)$$

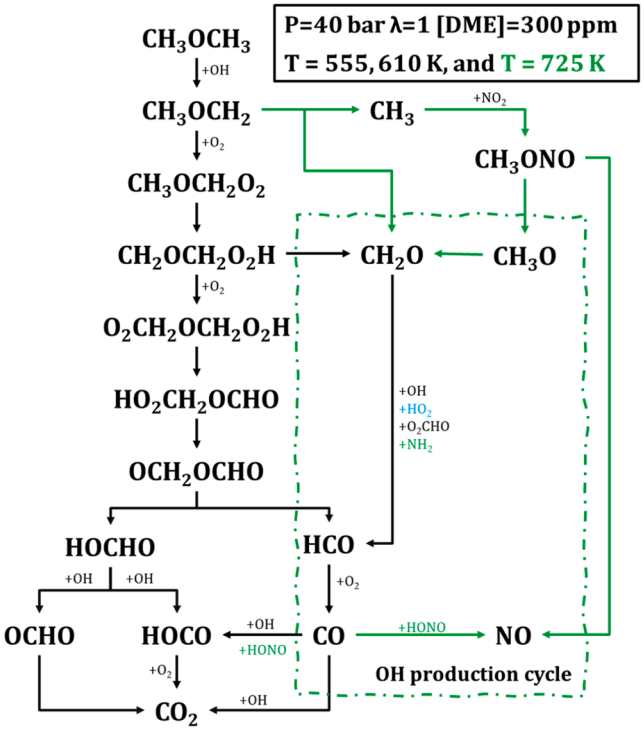

Fig. 11. Reaction path diagram for consumption of DME at $DME/NH_3 = 0.3$, stoichiometric ($\lambda = 1$) conditions at 40 bar for T = 555, 610 and 725 K. Sets 13 in Table 1.

Both reactions (r12) and (r13) constitute a competing pathway at intermediate temperatures that was mentioned by Burke et al. [25]. Once formed, $O_2CH_2OCH_2O_2H$ follows chain decomposition reactions, i.e. $O_2CH_2OCH_2O_2H \rightarrow HO_2CH_2OCHO \rightarrow OCH_2OCHO$, (r33 and r14, respectively) which represent the main OH production way in the low-temperature oxidation regime and the transition zone.

$$HO_2CH_2OCHO \rightleftharpoons OCH_2OCHO + OH \quad (r14)$$

$$O_2CH_2OCH_2O_2H \rightleftharpoons HO_2CH_2OCHO + OH \quad (r33)$$

In the transition zone between the low and high-temperature regimes, the formed CH_2O mainly consumes OH to form HCO (r34). It represents a competitive reaction with DME consumption. This reduces the available OH for its interaction with DME, thus decreasing the amount of CH_3OCH_2, which provokes the decomposition chain reactions to occur to a lesser extent, resulting in an overall decrease in DME conversion. CH_2O is an important intermediate product of the DME/NH_3 combustion that also appears for other mixtures as CH_3OH/NH_3 [e.g, 11].

The behavior in the transition zone (NTC) is overcome by increasing temperature, which provides other reaction pathways, such as the CH_3OCH_2 decomposition into CH_3 and CH_2O (r10), as reported in the literature [e.g. 17]. Subsequently, the CH_3 reacts with NO_2 producing CH_3ONO (r26) which leads to NO production (-r28), and finally, the NO leads to OH increase by its reaction with HO_2 (r25). Likewise, the production of NO by the reaction of CO with HONO (-r35) is also favored by the temperature increase.

$$CH_3OCH_2 \rightleftharpoons CH_3 + CH_2O \quad (r10)$$

$$NO + HO_2 \rightleftharpoons NO_2 + OH \quad (r25a)$$

$$CH_3 + NO_2 (+M) \rightleftharpoons CH_3ONO (+M) \quad (r26a)$$

$$CH_3O + NO (+M) \rightleftharpoons CH_3ONO (+M) \quad (r28a)$$

$$CH_2O + OH \rightleftharpoons HCO + H_2O \quad (r34)$$

$HOCO + NO \rightleftharpoons CO + HONO$ (r35)

Dai et al. [17] found that the DME + NO_2 reaction (r9) occurring during the conversion of DME/NH_3 mixtures was fast and significant under their experimental conditions, while we only found DME + OH (r5) to be important at high pressure, with a small contribution of DME + H/CH_3 (r36 and r37) at the lowest studied pressures. Dai et al. [17] reported $CH_3OCH_2O_2$ formation as a recombination of CH_3OCH_2 and O_2 (r31) under middle and high-pressure conditions, and the subsequent peroxide formation of $O_2CH_2OCH_2O_2H$ by O_2 addition (r13). However, under the present conditions studied, we only found the H-abstraction of DME by OH (r5) as an important consumption reaction of DME.

$CH_3OCH_3 + NO_2 \rightleftharpoons CH_3OCH_2 + HONO$ (r9)

$CH_3OCH_2 + O_2 \rightleftharpoons CH_3OCH_2O_2$ (r31a)

$CH_3OCH_3 + H \rightleftharpoons CH_3OCH_2 + H_2$ (r36)

$CH_3OCH_3 + CH_3 \rightleftharpoons CH_3OCH_2 + CH_4$ (r37)

The main reaction pathways always lead to CO_2 formation, including the reaction pathway appearing at high temperatures: $CH_3OCH_3 \rightarrow CH_3OCH_2 \rightarrow CH_3/CH_2O \rightarrow CH_3ONO \rightarrow CH_3O/NO$, which produces CO_2 and NO as final products. Similar finding was observed by Hashemi et al. [24] in their study of DME oxidation at high pressure (50 bar).

As for the NH_3 case, there are certain differences in the reaction path happening at atmospheric conditions as shown in Figure S6 in supplementary material, compared to the high-pressure conditions. One difference is that, under atmospheric pressure conditions, the CH_3OCH_2 consumption only happens by its dissociation into CH_2O and CH_3. Another difference is the apparition of the reaction path: $CH_3OCH_2 \rightarrow CH_3 \rightarrow C_2H_6 \rightarrow C_2H_5 \rightarrow C_2H_4 \rightarrow C_2H_3 \rightarrow CH_2O \rightarrow HCO \rightarrow CO \rightarrow CO_2$. NH_3 consumption is promoted by CH_3 at low pressure by the $CH_3 + NH_3 \rightleftharpoons CH_4 + NH_2$ (r38), but higher DME/NH_3 ratios provoke the increase of CH_3 radical concentration and therefore its recombination $CH_3 + CH_3$ (+M) $\rightleftharpoons C_2H_6$ (+M) (r39) can become significant.

As has been mentioned, products measured during the oxidation of DME/NH_3 mixtures are NO, NO_2, N_2O, N_2, H_2, HCN, CH_4, CO, and CO_2. N_2 and N_2O are the most abundant nitrogen species. NO appears only at 1 bar and NO_2 is also detected below 5 ppm under all studied experimental conditions (as has been mentioned above), which is consistent with the results of the previous works for pure NH_3 oxidation [4], and DME/NO oxidation mixtures [29].

Concentrations of N_2, N_2O, CO, and CO_2 as a function of temperature are shown in Figs. 12–15. Concentrations of other products (NO, CH_4, HCN, and H_2) are included in Figures S7 – S10 in the supplementary material.

Fig. 12 shows the N_2 formation under the studied experimental conditions, and the main nitrogen product of the NH_3 oxidation. Model calculations reproduce well the experimental trends.

Fig. 13 shows the N_2O production under the experimental conditions. There is a clear effect of pressure on the N_2O formed that leads to obtaining higher N_2O concentrations at higher pressures. Also, it is noticeable the effect of oxygen availability on N_2O production, increasing oxygen availability leads to an increased N_2O concentration, by a factor of 2-3, when switching from λ=1 to 3 at 40 bar for both DME/NH_3 ratios (0.05 and 0.3). The maximum N_2O concentrations, 100 and 128 ppm, are reached at 20 and 40 bar respectively, both for DME = 300 ppm and λ=3. This is lower than the N_2O amount reached for CH_4/NH_3 mixtures [9] (up to 290 ppm), for similar experimental conditions (λ=3, and 40 bar). The use of higher DME/NH_3 ratios can represent a disadvantage from a practical point of view compared with pure NH_3 since the addition of DME leads to the production of CH_3ONO which

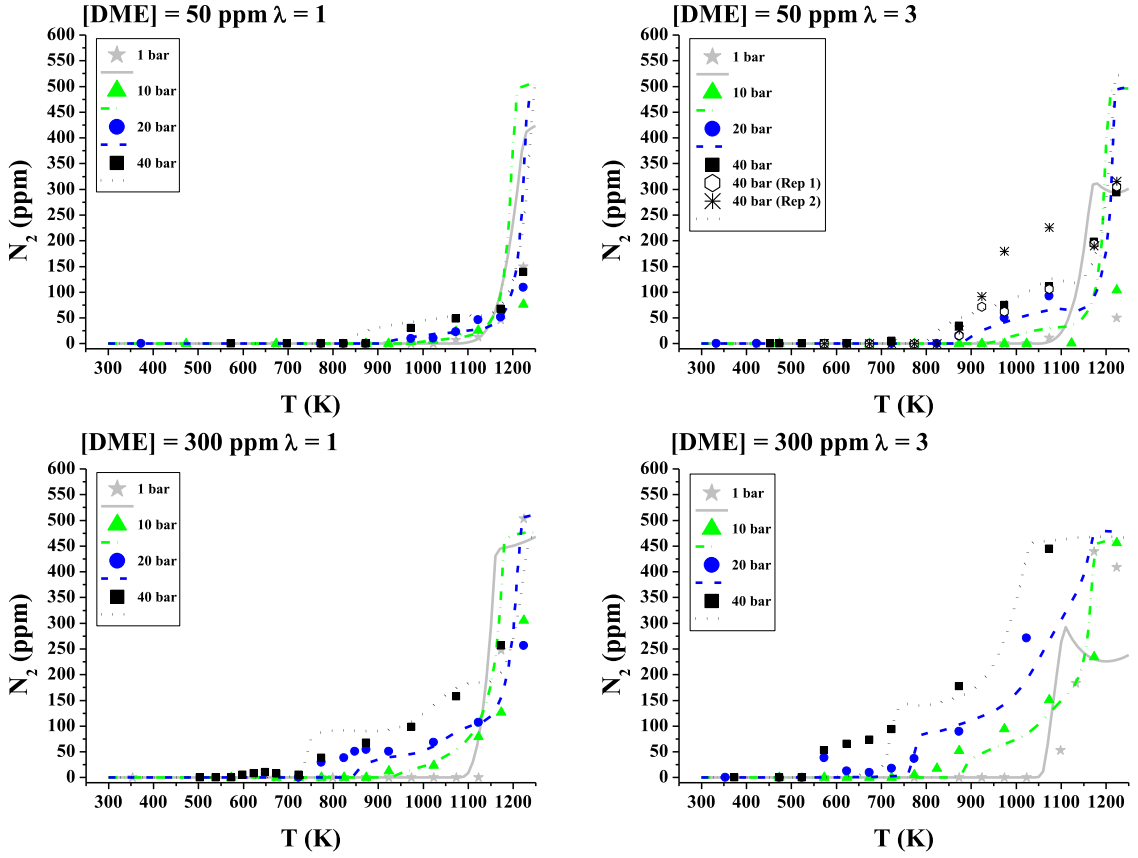

Fig. 12. N_2 conversion as a function of temperature for different pressures (1 - 40 bar). Sets 1-8 and 10-17 in Table 1. DME/NH_3 = 0.05 and 0.3, [NH_3] = 1000 ppm, λ = 1 and 3.

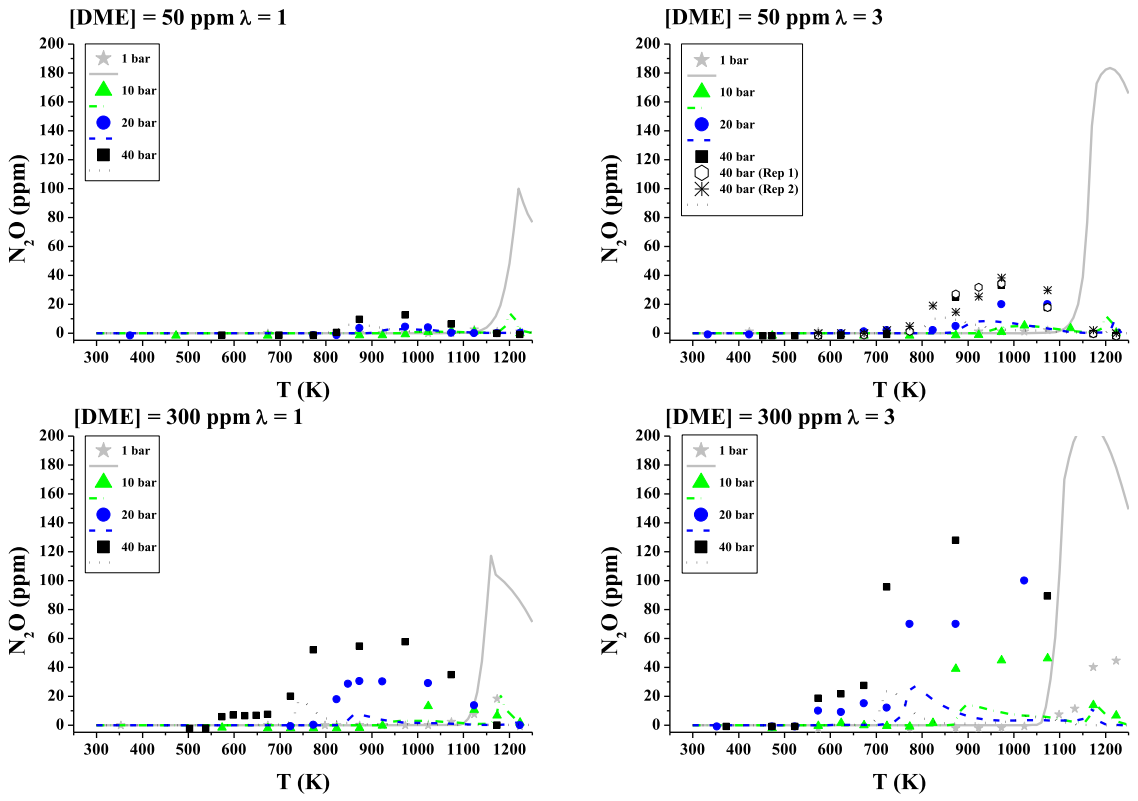

Fig. 13. N_2O conversion as a function of temperature for different pressures (1 - 40 bar). Sets 1-8 and 10-17 in Table 1. DME/NH_3 = 0.05 and 0.3, [NH_3] = 1000 ppm, λ = 1 and 3.

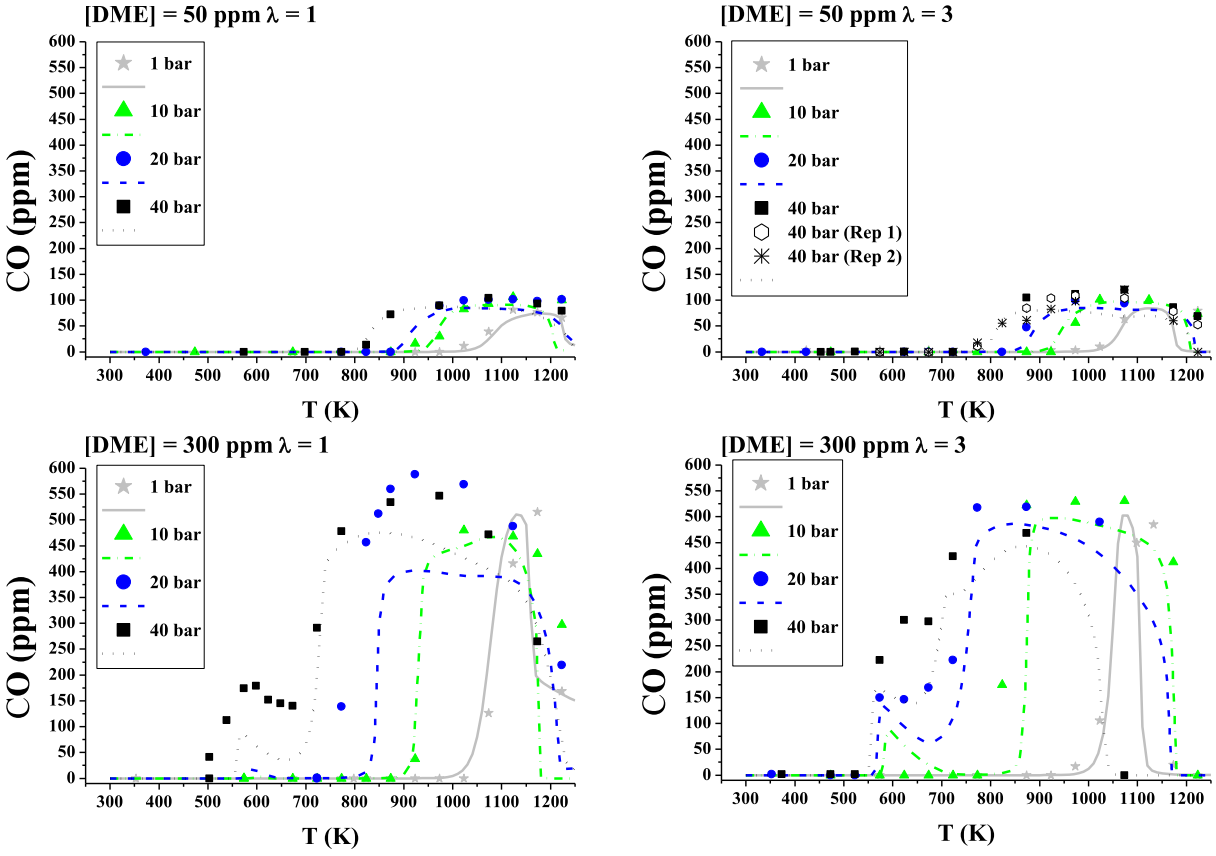

Fig. 14. CO production as a function of temperature for different pressures (1 - 40 bar). Sets 1-8 and 10-17 in Table 1. DME/NH_3 = 0.05 and 0.3, [NH_3] = 1000 ppm, λ = 1 and 3.

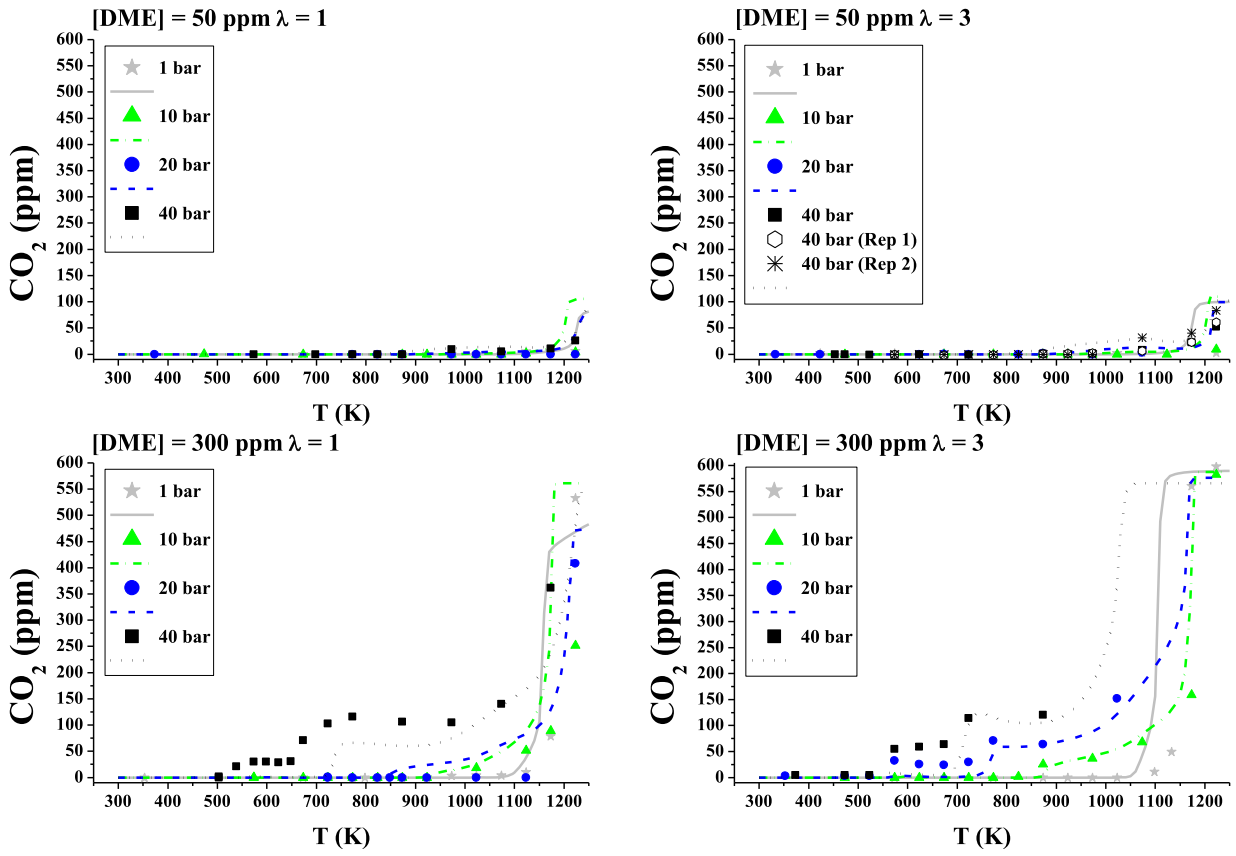

Fig. 15. CO_2 production as a function of temperature for different pressures (1 - 40 bar). Sets 1-8 and 10-17 in Table 1. DME/NH_3 = 0.05 and 0.3, [NH_3] = 1000 ppm, λ = 1 and 3.

decomposes to NO and this species reacts with NO_2 at high pressure to form N_2O.

Calculations show very low N_2O concentration under all studied conditions. However, the experimental concentrations are higher than the calculations as can be seen in Fig. 13. According to the model, the production of N_2O takes place through reaction (r40), as for CH_4/NH_3 mixtures [9], and it is consumed by reaction (r41).

$$NH_2 + NO_2 \rightleftharpoons N_2O + H_2O \quad \text{(r40)}$$

$$CO + N_2O \rightleftharpoons N_2 + CO_2 \quad \text{(r41)}$$

The CO production, as a function of temperature, is shown in Fig. 14. Calculations indicate that CO is mainly produced by reaction (r42), under the studied conditions.

$$HCO + O_2 \rightleftharpoons CO + HO_2 \quad \text{(r42)}$$

The NTC behavior is also noted in the CO experimental data, Fig. 14. CO is consumed by its reaction with HONO and OH to form HOCO and CO_2 (-r35, r43, and r44). The model captures the main trend of CO production.

$$HOCO + NO \rightleftharpoons CO + HONO \quad \text{(r35a)}$$

$$CO + OH \rightleftharpoons CO_2 + H \quad \text{(r43)}$$

$$CO + OH \rightleftharpoons HOCO \quad \text{(r44)}$$

The CO_2 production as a function of temperature is shown in Fig. 15. Its production occurs mainly through (r43) and in a minor extent through (r45) and (r46).

$$HCO + NO_2 \rightleftharpoons NO + CO_2 + H \quad \text{(r45)}$$

$$HOCO + O_2 \rightleftharpoons CO_2 + HO_2 \quad \text{(r46)}$$

Experimental results show that CH_4 is mostly produced for the highest DME/NH_3 ratio. Figure S8 shows the CH_4 production as a function of temperature and the model reproduces well the main experimental trends. The formation of CH_4 decreases with increasing pressure. CH_4 is mainly formed in reactions (r37), (-r47), and (r48) while consumption mainly occurs by reaction (r49).

$$CH_3OCH_3 + CH_3 \rightleftharpoons CH_3OCH_2 + CH_4 \quad \text{(r37a)}$$

$$CH_4 + O_2 \rightleftharpoons CH_3 + HO_2 \quad \text{(r47)}$$

$$CH_2O + CH_3 \rightleftharpoons HCO + CH_4 \quad \text{(r48)}$$

$$CH_4 + OH \rightleftharpoons CH_3 + H_2O \quad \text{(r49)}$$

HCN production is found to have a similar behavior to NO, being only produced at the lowest pressure studied, and Figure S9 shows the results of HCN production as a function of temperature. HCN is produced from the interaction between NH_3 and DME at higher temperatures (about 1100-1200 K) compared to what happens during the oxidation of CH_4/NH_3 mixtures [9]. The model underpredicts the concentration of HCN.

H_2 production is favored by low pressure and higher DME/NH_3 ratios, and an example of H_2 production results is included in Figure S10 as a function of temperature for experimental results of sets 1-8 and 10-17 in Table 1. The model reproduces well the main experimental trends

Sensitivity analyses were performed for given conditions. Fig. 16 shows reactions to which the NH_3 concentrations are most sensitive, for DME/NH_3 = 0.3, at 40 bar and λ = 1 at 555, 610, and 725 K as an example. The results show that NH_3 consumption is promoted by: the reaction of DME with OH, NH_2, O_2CHO, and HO_2 to form CH_3OCH_2 radicals, by the decomposition of HO_2CH_2OCHO to produce OCH_2OCHO and OH (r14) radicals, and by the oxidation of $CH_2OCH_2O_2H$ to form

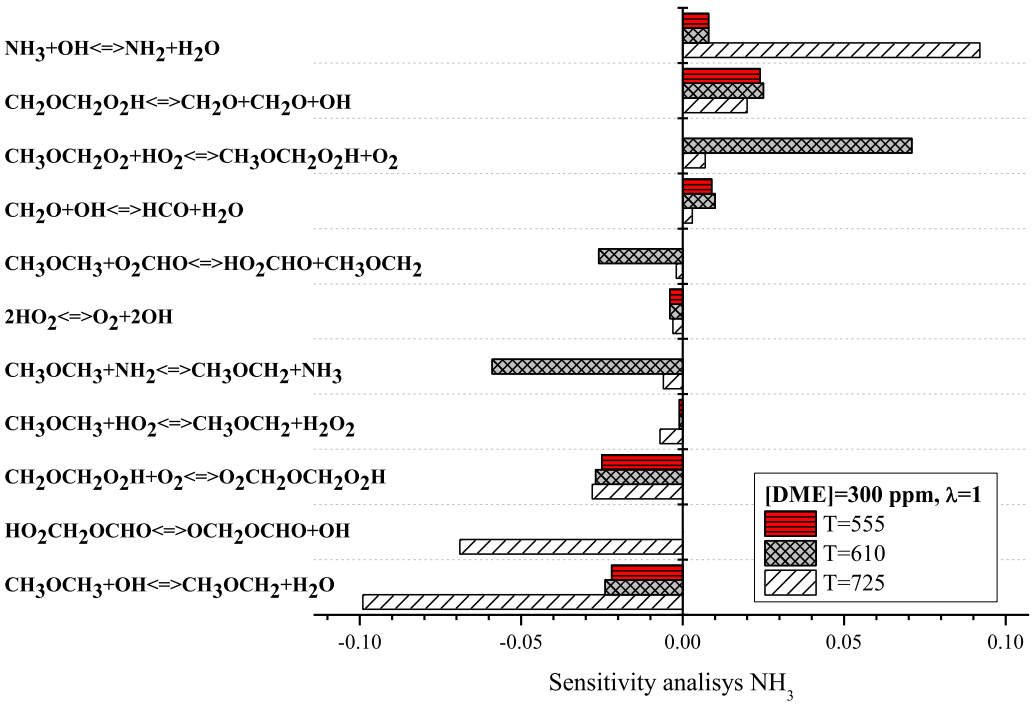

Fig. 16. Sensitivity analysis of NH_3 at different temperatures (555, 610, and 725 K) and 40 bar. Sets 13 in Table 1. DME/NH_3 = 0.3, [NH_3] = 1000 ppm, and λ = 1.

$O_2CH_2OCH_2O_2H$ (r13). For the same experimental conditions, NH_3 conversion is inhibited by the reaction of $CH_3OCH_2O_2$ with HO_2, and the $CH_2OCH_2O_2H$ decomposition to produce CH_2O followed by its reaction with OH producing HCO and H_2O. The reaction of NH_3 H-abstraction via OH to form NH_2 and H_2O appears to be one of the most sensitive.

Fig. 17 shows the sensitivity analysis for DME under the same experimental conditions as Fig. 16 (DME/NH_3 = 0.3, 40 bar, and λ = 1 at 555, 610, and 725 K). The results indicate that DME consumption is promoted by its reaction with OH and HO_2 to form CH_3OCH_2 radicals, by the decomposition of HO_2CH_2OCHO to produce OCH_2OCHO and OH radicals, and by the oxidation of $CH_2OCH_2O_2H$ to form O_2CH_2O-CH_2O_2H, as well as in the NH_3 case. The most inhibitory reactions are the reaction of NH_3 with OH to form NH_2, and the decomposition of $CH_2OCH_2O_2H$ into CH_2O followed by its reaction with OH producing HCO and H_2O, as happened in the NH_3 case, which coincides with what was observed in earlier works [18,87].

5. Conclusions

The present experimental and modeling study contains the main

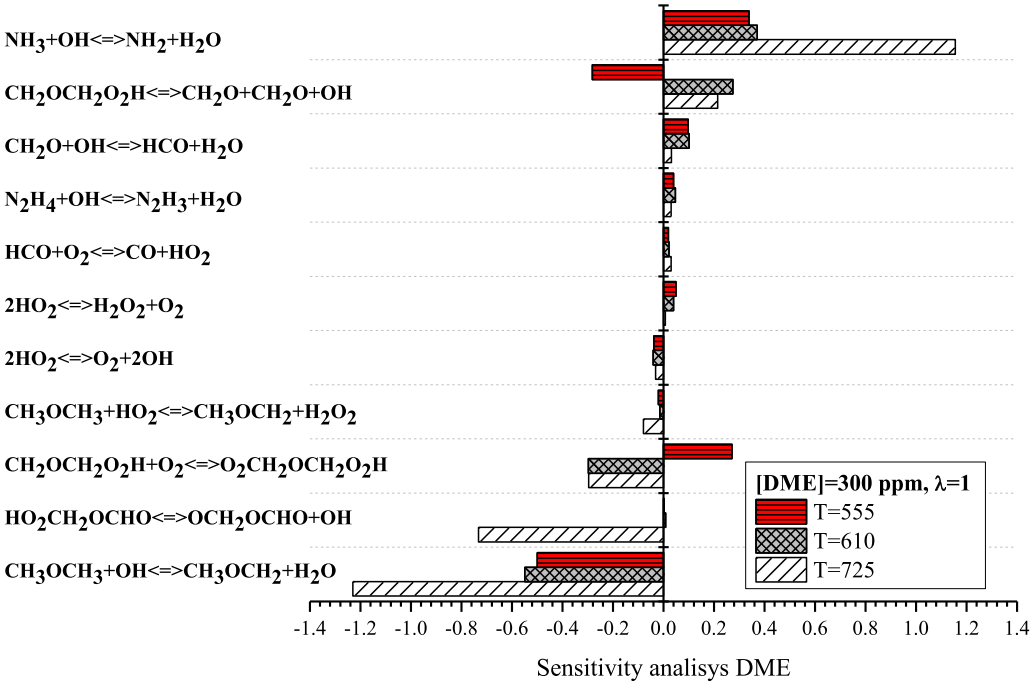

Fig. 17. DME sensitivity analysis at different temperatures (555, 610, and 725 K) and 40 bar. Sets 13 in Table 1. DME/NH_3 = 0.3, [NH_3] = 1000 ppm, and λ = 1.

features of DME/NH_3 mixtures oxidation in a quartz tubular flow reactor with argon as a bath gas, under reducing, stoichiometric, and oxidizing conditions, from 1 to 40 bar of pressure and considering a temperature range of 350 K–1225 K.

The main product of ammonia oxidation is N_2 with minor amounts of N_2O formed, while HCN and NO are only produced under certain conditions (DME/NH_3 = 0.3 and atmospheric conditions). NO_2 formation is negligible under all studied conditions.

High pressure acts to favor the formation of N_2 and CO_2 from the DME/NH_3 mixture and avoids the HCN and NO production at high DME/NH_3 ratios, compared to atmospheric pressure. This is a positive outcome of working under high pressure. However, high pressure tends to power N_2O production, especially at high DME/NH_3 ratios.

Oxygen availability represents a key factor in the combustion of DME/NH_3 mixtures. While the onset temperature of the reaction hardly changes when varying the oxygen concentration, the ammonia, and DME full conversion takes place at lower temperatures when higher concentrations of oxygen are used.

In certain conditions, the DME performs well as a NH_3 combustion promotor, reducing the NH_3 onset temperature for conversion initiation. Also, compared with CH_4 and H_2 as additives, DME shows a better performance. This is another indication of the good performance of DME as an additive.

In the present work, the chemical kinetic mechanism used in previous works by our group [8,9] has been extended and updated with literature works, to capture the main trends of DME/NH_3 oxidation at high pressure. The main challenge was to consider the C-N interactions that seem to be present in the combustion of DME/NH_3 mixtures. The updated mechanism shows good agreement with experimental results (both from the present work and the literature) for both NH_3 and DME conversion under all the studied conditions. Nevertheless, some discrepancies have been found in the N_2O and HCN predictions, indicating that there is still room for improvement.

The transition zone behavior (NTC) is more noticeable with higher DME ratios. Model calculations indicate that this phenomenon is produced by the formation of CH_2O which competes with DME for OH radicals, and it is overcome by the effect of temperature, which provokes the CH_3OCH_2 decomposition, which leads to OH production.

The reaction of DME with NH_2, OH, O_2CHO, and HO_2 to form CH_3OCH_2 radicals, the decomposition of HO_2CH_2OCHO to produce OCH_2OCHO and OH radicals, and the oxidation of $CH_2OCH_2O_2H$ promote the consumption of NH_3 and DME. On the counterpart, the reaction of $CH_3OCH_2O_2$ with HO_2, and the decomposition of $CH_2OCH_2O_2H$ to produce CH_2O followed by its reaction with OH producing HCO and H_2O are the major inhibition reactions of NH_3 and DME consumption. The reaction of NH_3 with OH to form NH_2 and H_2O appears as a very sensitive reaction.

Acknowledgments

The authors acknowledge the funding from MINECO and FEDER (Projects TED2021-129557B-I00 and PID2021-124032OB-I00) and MINECO PRE2019-090162 for financial support, and the Aragón Government (Ref. T22_23R), co-funded by FEDER 2021-2027 "Construyendo Europa desde Aragón ".

Supplementary materials

Supplementary material associated with this article can be found, in the online version, at doi:10.1016/j.combustflame.2024.113875.

References

[1] A. Valera-Medina, F. Amer-Hatem, A.K. Azad, I.C. Dedoussi, M. De Joannon, R. X. Fernandes, P. Glarborg, H. Hashemi, X. He, S. Mashruk, J. McGowan, C. Mounaim-Rouselle, A. Ortiz-Prado, A. Ortiz-Valera, I. Rossetti, B. Shu, M. Yehia, H. Xiao, M. Costa, Review on ammonia as a potential fuel: From synthesis to economics, Energy Fuels 35 (2021) 6964–7029.
[2] M.U. Alzueta, M. Abián, I. Elvira, V.D. Mercader, L. Sieso, Unraveling the NO reduction mechanisms occurring during the combustion of NH_3/CH_4 mixtures, Combust. Flame. 257 (2023) 112531.
[3] H. Kobayashi, A. Hayakawa, K.D.K.A. Somarathne, E.C. Okafor, Science and technology of ammonia combustion, Proc. Combust. Inst. 37 (2019) 109–133.
[4] P. García-Ruiz, M. Uruén, M. Abián, M.U. Alzueta, High pressure ammonia oxidation in a flow reactor, Fuel 348 (2023) 128302.
[5] Y. Song, H. Hashemi, J.M. Christensen, C. Zou, P. Marshall, P. Glarborg, Ammonia oxidation at high pressure and intermediate temperatures, Fuel 181 (2016) 358–365.
[6] L. Dai, S. Gersen, P. Glarborg, H. Levinsky, A. Mokhov, Experimental and numerical analysis of the autoignition behavior of NH_3 and NH_3/H_2 mixtures at high pressure, Combust. Flame. 215 (2020) 134–144.
[7] M.U. Alzueta, V. Mercader, A. Cuoci, S. Gersen, H. Hashemi, P. Glarborg, Flow reactor oxidation of ammonia-hydrogen fuel mixtures, Energy Fuels 38 (2024) 3369–3381.
[8] P. García-Ruiz, D. Castejón, M. Abengochea, R. Bilbao, M.U. Alzueta, High-pressure study of the conversion of NH_3/H_2 mixtures in a flow reactor, Proc. Combust. Inst. 40 (2024) 105726.
[9] P. García-Ruiz, I. Salas, E. Casanova, R. Bilbao, M.U. Alzueta, Experimental and modeling high-pressure study of ammonia-methane oxidation in a flow reactor, Energy and Fuels 38 (2024) 1399–1415.
[10] L. Dai, S. Gersen, P. Glarborg, A. Mokhov, H. Levinsky, Autoignition studies of NH_3/CH_4 mixtures at high pressure, Combust. Flame. 218 (2020) 19–26.
[11] Y. Zhuang, R. Wu, X. Wang, R. Zhai, C. Gao, An experimental and modeling study on the oxidation of ammonia-methanol mixtures in a jet stirred reactor, Fuel 356 (2024) 129628.
[12] Z. Wang, X. Han, Y. He, R. Zhu, Y. Zhu, Z. Zhou, K. Cen, Experimental and kinetic study on the laminar burning velocities of NH_3 mixing with CH_3OH and C_2H_5OH in premixed flames, Combust. Flame. 229 (2021) 111392.
[13] L. Cai, F. Vom Lehn, H. Pitsch, Higher alcohol and ether biofuels for compression-ignition engine application: A review with emphasis on combustion kinetics, Energy and Fuels 35 (2021) 1890–1917.
[14] A. Omari, B. Heuser, S. Pischinger, C. Rüdinger, Potential of long-chain oxymethylene ether and oxymethylene ether-diesel blends for ultra-low emission engines, Appl. Energy. 239 (2019) 1242–1249.
[15] P. Soltic, T. Hilfiker, Y. Wright, G. Hardy, B. Fröhlich, D. Klein, The potential of dimethyl ether (DME) to meet current and future emissions standards in heavy-duty compression-ignition engines, Fuel 355 (2024) 129357.
[16] A. Valera-Medina, H. Xiao, M. Owen-Jones, W.I.F. David, P.J. Bowen, Ammonia for power, Prog. Energy Combust. Sci 69 (2018) 63–102.
[17] L. Dai, H. Hashemi, P. Glarborg, S. Gersen, P. Marshall, A. Mokhov, H. Levinsky, Ignition delay times of NH_3/DME blends at high pressure and low DME fraction: RCM experiments and simulations, Combust. Flame. 227 (2021) 120–134.
[18] G. Issayev, B.R. Giri, A.M. Elbaz, K.P. Shrestha, F. Mauss, W.L. Roberts, A. Farooq, Ignition delay time and laminar flame speed measurements of ammonia blended with dimethyl ether: A promising low carbon fuel blend, Renew. Energy. 181 (2022) 1353–1370.
[19] X. Jiang, Q. Zhang, X. Liu, T. Zhang, Y. Zhang, Z. Huang, F. Deng, N. Zhao, H. Zheng, Y. Yan, A shock tube study of the ignition delay time of DME/ammonia mixtures: Effect of fuel blending from high temperatures to the NTC regime, Fuel 367 (2024) 131426.
[20] K. Moshammer, A.W. Jasper, D.M. Popolan-Vaida, A. Lucassen, P. Diévart, H. Selim, A.J. Eskola, C.A. Taatjes, S.R. Leone, S.M. Sarathy, Y. Ju, P. Dagaut, K. Kohse-Höinghaus, N. Hansen, Detection and Identification of the keto-hydroperoxide ($HOOCH_2OCHO$) and other intermediates during low-temperature oxidation of dimethyl ether, J. Phys. Chem. A. 119 (2015) 7361–7374.
[21] A. Stagni, S. Schmitt, M. Pelucchi, A. Frassoldati, K. Kohse-Höinghaus, T. Faravelli, Dimethyl ether oxidation analyzed in a given flow reactor: Experimental and modeling uncertainties, Combust. Flame. 240 (2022) 111998.
[22] S. Zhu, Q. Xu, R. Tang, J. Gao, Z. Wang, J. Pan, D. Zhang, A comparative study of oxidation of pure ammonia and ammonia/dimethyl ether mixtures in a jet-stirred reactor using SVUV-PIMS, Combust. Flame. 250 (2023) 112643.
[23] L. Marrodán, Á. Millera, R. Bilbao, M.U. Alzueta, An experimental and modeling study of acetylene-dimethyl ether mixtures oxidation at high-pressure, Fuel 327 (2022) 125143.
[24] H. Hashemi, J.M. Christensen, P. Glarborg, High-pressure pyrolysis and oxidation of DME and DME/CH_4, Combust. Flame. 205 (2019) 80–92.
[25] U. Burke, K.P. Somers, P. O'Toole, C.M. Zinner, N. Marquet, G. Bourque, E. L. Petersen, W.K. Metcalfe, Z. Serinyel, H.J. Curran, An ignition delay and kinetic modeling study of methane, dimethyl ether, and their mixtures at high pressures, Combust. Flame. 162 (2015) 315–330.
[26] M.U. Alzueta, J. Muro, R. Bilbao, P. Glarborg, Oxidation of dimethyl ether and its interaction with nitrogen oxides, Isr. J. Chem. 39 (1999) 73–86.
[27] H. Zhang, S. Schmitt, L. Ruwe, K. Kohse-Höinghaus, Inhibiting and promoting effects of NO on dimethyl ether and dimethoxymethane oxidation in a plug-flow reactor, Combust. Flame. 224 (2021) 94–107.
[28] L. Marrodán, Á.J. Arnal, Á. Millera, R. Bilbao, M.U. Alzueta, The inhibiting effect of NO addition on dimethyl ether high-pressure oxidation, Combust. Flame. 197 (2018) 1–10.
[29] M. Pelucchi, S. Schmitt, N. Gaiser, A. Cuoci, A. Frassoldati, H. Zhang, A. Stagni, P. Oßwald, K. Kohse-Höinghaus, T. Faravelli, On the influence of NO addition to dimethyl ether oxidation in a flow reactor, Combust. Flame. 257 (2022) 112464.

[30] X. Shi, W. Li, J. Zhang, Q. Fang, Y. Zhang, Z. Xi, Y. Li, Exploration of NH_3 and NH_3/DME laminar flame propagation in O_2/CO_2 atmosphere: Insights into NH_3/CO_2 interactions, Combust. Flame. 260 (2024) 113245.

[31] M. Yu, G. Luo, R. Sun, W. Qiu, L. Chen, L. Wang, Z. Hu, X. Li, H. Yao, Experimental and numerical study on emission characteristics of NH_3/DME/air flames in a premixed burner, Combust. Flame. 259 (2024) 113098.

[32] Y. Murakami, H. Nakamura, T. Tezuka, K. Hiraoka, K. Maruta, Effects of mixture composition on oxidation and reactivity of DME/NH_3/air mixtures examined by a micro flow reactor with a controlled temperature profile, Combust. Flame. 238 (2022) 111911.

[33] L. Dai, S. Gersen, P. Glarborg, H. Levinsky, A. Mokhov, Experimental and numerical analysis of the autoignition behavior of NH_3 and NH_3/H_2 mixtures at high pressure, Combust. Flame. 215 (2020) 134–144.

[34] K.P. Shrestha, S. Eckart, A.M. Elbaz, B.R. Giri, C. Fritschen, L. Seidel, W.L. Roberts, H. Krause, F. Mauss, A comprehensive kinetic model for dimethyl ether and dimethoxymethane oxidation and NO_x interaction utilizing experimental laminar flame speed measurements at elevated pressure and temperature, Combust. Flame. 218 (2020) 57–74.

[35] X. Meng, M. Zhang, C. Zhao, H. Tian, J. Tian, W. Long, M. Bi, Study of combustion and NO chemical reaction mechanism in ammonia blended with DME, Fuel 319 (2022) 123832.

[36] H. Xiao, H. Li, Experimental and kinetic modeling study of the laminar burning velocity of NH_3/DME/air premixed flames, Combust. Flame. 245 (2022) 112372.

[37] X. Meng, L. Liu, M. Zhang, X. Zhang, W. Long, M. Bi, Chemical kinetic and behavior study of the cracked gas of H_2/N_2 and DME addition on ammonia combustion in lean-burn condition, Int. J. Hydrogen Energy. 49 (2024) 997–1008.

[38] G. Yin, J. Li, M. Zhou, J. Li, C. Wang, E. Hu, Z. Huang, Experimental and kinetic study on laminar flame speeds of ammonia/dimethyl ether/air under high temperature and elevated pressure, Combust. Flame. 238 (2022) 111915.

[39] W. Li, Q. Fang, J. Zhang, Y. Chow, L. Ye, Y. Li, Role of CH_2O moiety on laminar burning velocities of oxymethylene ethers (OME_n): A case study of dimethyl ether, OME_1 and OME_2, Proc. Combust. Inst. 39 (2023) 795–804.

[40] J.M. Colóm-Díaz, Á. Millera, R. Bilbao, M.U. Alzueta, High pressure study of H_2 oxidation and its interaction with NO, Int. J. Hydrogen Energy. 44 (2019) 6325–6332.

[41] Ansys Chemkin-Pro Chemical Kinetics Simulation Software, Chemkin ANSYS, San Diego, 2023.

[42] P. Glarborg, J.A. Miller, B. Ruscic, S.J. Klippenstein, Modeling nitrogen chemistry in combustion, Prog. Energy Combust. Sci. 67 (2018) 31–68.

[43] M.U. Alzueta, M. Guerrero, Á. Millera, P. Marshall, P. Glarborg, Experimental and kinetic modeling study of oxidation of acetonitrile, Proc. Combust. Inst. 38 (2021) 575–583.

[44] P. Glarborg, C.S. Andreasen, H. Hashemi, R. Qian, P. Marshall, Oxidation of methylamine, Int. J. Chem. Kinet. 52 (2020) 893–906.

[45] L. Marrodán, T. Pérez, M.U. Alzueta, Conversion of methylamine in a flow reactor and its interaction with NO, Combust. Flame. 259 (2024) 113130.

[46] M.P. Burke, S.J. Klippenstein, Ephemeral collision complexes mediate chemically termolecular transformations that affect system chemistry, Nat. Chem. 9 (2017) 1078–1082.

[47] S.J. Klippenstein, R. Sivaramakrishnan, U. Burke, K.P. Somers, H.J. Curran, L. Cai, H. Pitsch, M. Pelucchi, T. Faravelli, P. Glarborg, $H\dot{O}_2 + H\dot{O}_2$: High level theory and the role of singlet channels, Combust. Flame. 243 (2022) 111975.

[48] P. Marshall, G. Rawling, P. Glarborg, New reactions of diazene and related species for modelling combustion of amine fuels, Mol. Phys. 119 (2021) 1–28.

[49] M.U. Alzueta, L. Ara, V.D. Mercader, M. Delogu, R. Bilbao, Interaction of NH_3 and NO under combustion conditions. Experimental flow reactor study and kinetic modeling simulation, Combust. Flame. 235 (2022) 111691.

[50] M.U. Alzueta, I. Salas, H. Hashemi, P. Glarborg, CO assisted NH_3 oxidation, Combust. Flame 257 (2022) 112438.

[51] P. Glarborg, H. Hashemi, S. Cheskis, A.W. Jasper, On the rate constant for $NH_2 + HO_2$ and third-body collision efficiencies for $NH_2 + H$ (+M) and $NH_2 + NH_2$ (+M), J. Phys. Chem. A. 125 (2021) 1505–1516.

[52] P. Glarborg, H. Hashemi, P. Marshall, Challenges in kinetic modeling of ammonia pyrolysis, Fuel Commun 10 (2022) 100049.

[53] P. Glarborg, The $NH_3/NO_2/O_2$ system: Constraining key steps in ammonia ignition and N_2O formation, Combust. Flame. 2 (2022) 112311.

[54] S.J. Klippenstein, P. Glarborg, Theoretical kinetics predictions for $NH_2 + HO_2$, Combust. Flame. 236 (2022) 111787.

[55] A. Stagni, C. Cavallotti, H-abstractions by O_2, NO_2, NH_2, and HO_2 from H_2NO: Theoretical study and implications for ammonia low-temperature kinetics, Proc. Combust. Inst. 39 (2023) 633–641.

[56] L. Marrodán, Á. Millera, R. Bilbao, M.U. Alzueta, High-pressure study of methyl formate oxidation and its interaction with NO, Energy and Fuels 28 (2014) 6107–6115.

[57] P. Glarborg, M.U. Alzueta, K. Dam-Johansen, Kinetic modeling of hydrocarbon/nitric oxide interactions in a flow reactor, Combust. Flame. 115 (1998) 1–27.

[58] C.L. Rasmussen, J. Hansen, P. Marshall, P. Glarborg, Experimental measurements and kinetic modeling of $CO/H_2/O_2/NO_x$ conversion at high pressure, Int. J. Chem. Kinet. 40 (2008) 454–480.

[59] C.L. Rasmussen, J.G. Jakobsen, P. Glarborg, Experimental measurements and kinetic modeling of CH_4/O_2 and $CH_4/C_2H/O_2$ conversion at high pressure, Int. J. Chem. Kinet. 40 (2008) 778–807.

[60] C.L. Rasmussen, K.H. Wassard, K. Dam-Johansen, P. Glarborg, Methanol oxidation in a flow reactor: Implications for the branching ratio of the $CH_3OH + OH$ reaction, Int. J. Chem. Kinet. 40 (2008) 423–441.

[61] C.L. Rasmussen, A.E. Rasmussen, P. Glarborg, Sensitizing effects of NO_x on CH_4 oxidation at high pressure, Combust. Flame. 154 (2008) 529–545.

[62] J. Giménez-López, C.T. Rasmussen, H. Hashemi, M.U. Alzueta, Y. Gao, P. Marshall, C.F. Goldsmith, P. Glarborg, Experimental and kinetic modeling study of C_2H_2 oxidation at high pressure, Int. J. Chem. Kinet. 48 (2016) 724–738.

[63] M.U. Alzueta, M. Borruey, A. Callejas, Á. Millera, R. Bilbao, An experimental and modeling study of the oxidation of acetylene in a flow reactor, Combust. Flame. 152 (2008) 377–386.

[64] P. Marshall, P. Glarborg, Ab initio and kinetic modeling studies of formic acid oxidation, Proc. Combust. Inst. 35 (2015) 153–160.

[65] L. Marrodán, E. Royo, Á. Millera, R. Bilbao, M.U. Alzueta, High pressure oxidation of dimethoxymethane, Energy and Fuels 29 (2015) 3507–3517.

[66] L. Marrodán, Á.J. Arnal, Á. Millera, R. Bilbao, M.U. Alzueta, High-pressure ethanol oxidation and its interaction with NO, Fuel 223 (2018) 394–400.

[67] L. Marrodán, L. Berdusán, V. Aranda, Á. Millera, R. Bilbao, M.U. Alzueta, Influence of dimethyl ether addition on the oxidation of acetylene in the absence and presence of NO, Fuel 183 (2016) 1–8.

[68] Y. Song, R. Liu, Y. Guan, J. Gao, J. Lou, H. Ma, J. Song, Computational study of the reaction of dimethyl ether with nitric oxide. Mechanism and kinetic modeling, J. Phys. Chem. A. 123 (2019) 26–36.

[69] Y. Guan, R. Liu, J. Lou, H. Ma, J. Song, Computational investigation on the reaction of dimethyl ether with nitric dioxide. II. Detailed chemical kinetic modeling, Theor. Chem. Acc. 139 (2020) 1–12.

[70] A.J. Eskola, S.A. Carr, R.J. Shannon, B. Wang, M.A. Blitz, M.J. Pilling, P. W. Seakins, Analysis of the kinetics and yields of OH radical production from the $CH_3OCH_2 + O_2$ reaction in the temperature range 195-650 K: An experimental and computational study, J. Phys. Chem. A. 118 (2014) 6773–6788.

[71] V. Samu, T. Varga, I. Rahinov, S. Cheskis, T. Turányi, Determination of rate parameters based on NH_2 concentration profiles measured in ammonia-doped methane–air flames, Fuel 212 (2018) 679–683.

[72] R.S. Tranter, R.W. Walker, Rate constants for the reactions of H atoms and OH radicals with ethers at 753 K, Phys. Chem. Chem. Phys. 3 (2001) 4722–4732.

[73] R.D. Cook, D.F. Davidson, R.K. Hanson, High-Temperature shock tube measurements of dimethyl ether decomposition and the reaction of dimethyl ether with OH, J. Phys. Chem. A. 113 (2009) 9974–9980.

[74] C. Bänsch, J. Kiecherer, M. Szöri, M. Olzmann, Reaction of dimethyl ether with hydroxyl radicals: Kinetic isotope effect and prereactive complex formation, J. Phys. Chem. A. 117 (2013) 8343–8351.

[75] S.A. Carr, T.J. Still, M.A. Blitz, A.J. Eskola, M.J. Pilling, P.W. Seakins, R. J. Shannon, B. Wang, S.H. Robertson, Experimental and theoretical study of the kinetics and mechanism of the reaction of OH radicals with dimethyl ether, J. Phys. Chem. A. 117 (2013) 11142–11154.

[76] D.J. McKenney, B.W. Wojciechowski, K.J. Laidler, Kinetics and mechanisms of the pyrolysis of dimethyl ether. II. The reaction inhibited by nitric oxide and propylene, Can. J. Chem. 41 (1963) 1993–2008.

[77] P. Dagaut, J. Lucheke, M. Cathonnet, The low temperature oxidation of DME and mutual sensitization of the oxidation of DME and nitric oxide: experimental and detailed kinetic modeling, Combust. Sci. Technol. 165 (2001) 61–84.

[78] W. Ye, J.C. Shi, R.T. Zhang, X.J. Wu, X. Zhang, M.L. Qi, S.N. Luo, Experimental and kinetic modeling study of CH_3OCH_3 ignition sensitized by NO_2, Energy Fuels 30 (2016) 10900–10908.

[79] Y.L. Shang, J.C. Shi, L.M. Fang, Q.G. Feng, H.Y. Wang, S.N. Luo, Theoretical investigation on hydrogen abstraction by NO_2 from symmetric ethers $(CH_3)_{2x}O$ (x=1-4), J. Phys. Chem. A. 122 (2018) 6829–6841.

[80] J. Gao, G. Yulei, L. Junpeng, M. Haixia, S. Jirong, Kinetic modeling for unimolecular β-scission of the methoxymethyl radical from quantum chemical and RRKM analyses, Combust. Flame. 197 (2018) 243–253.

[81] J. Sehested, K. Sehested, J. Platz, H. Egsgaard, O.J. Nielsen, Oxidation of dimethyl ether: Absolute rate constants for the self reaction of CH_3OCH_2 radicals, the reaction of CH_3OCH_2 radicals with O_2, and the thermal decomposition of CH_3OCH_2 radicals, Int. J. Chem. Kinet. 29 (1997) 627–636.

[82] Q.S. Li, R.H. Lu, Direction dynamics study of the hydrogen abstraction reaction $CH_2O + NH_2 \rightarrow CHO + NH_3$, J. Phys. Chem. A. 106 (2002) 9446–9450.

[83] A. Stagni, C. Cavallotti, S. Arunthanayothin, Y. Song, O. Herbinet, F. Battin-Leclerc, T. Faravelli, An experimental, theoretical and kinetic-modeling study of the gas-phase oxidation of ammonia, React. Chem. Eng. 5 (2020) 696–711.

[84] E.W.G. Diau, T.L. Tso, Y.P. Lee, Kinetics of the reaction hydroxyl + ammonia in the range 273-433 K, J. Phys. Chem. 94 (1990) 5261–5265.

[85] M. Abián, M. Benés, A. de Goñi, B. Muñoz, M.U. Alzueta, Study of the oxidation of ammonia in a flow reactor. Experiments and kinetic modeling simulation, Fuel 300 (2021) 120979.

[86] S. Salimian, R.K. Hanson, C.H. Kruger, High temperature study of the reactions of O and OH with NH_3, Int. J. Chem. Kinet. 16 (1984) 725–739.

[87] W. Guan, A. Abdelsamie, C. Chi, Z. He, D. Thévenin, A dedicated reduced kinetic model for ammonia/dimethyl-ether turbulent premixed flames, Combust. Flame. 257 (2023) 113002.